201

MEASUREMENT OF THE LOWER EXPLOSIVE LIMIT OF COMBUSTIBLE DUST CLOUDS IN A 20-LITRE SPHERICAL CHAMBER

by

DAVID LEE SIDEBOTTOM

B.S., Kansas State University, 1983

A MASTER'S THESIS

submitted in partial fulfillment of the

requirements for the degree

MASTER OF SCIENCE

Department of Physics

KANSAS STATE UNIVERSITY
Manhattan, Kansas

1985

Approved by:

Major Professor

LD
2668
.T4
1985
S562
c.2

A11202 985265

TABLE OF CONTENTS

INTRODUCTION	1
THEORY	5
CONCENTRATION MEASUREMENT	12
PARTICLE SIZE MEASUREMENT	17
STATISTICS of EXPLOSION TESTING	17
APPARATUS	23
EXPERIMENT	40
PROCEDURE	47
SAMPLE PREPARATION	48
RESULTS and DISCUSSION	48
A. Error	49
B. Particle Size Analysis	65
C. Cloud Uniformity	66
D. Concentration Measurements	66
E. Prediction of L.E.L. vs. Particle Size	71
SUMMARY	80
TABLES	81
REFERENCES	93
APPENDIX	95

LIST OF TABLES

Table 1a: Preliminary Sweep of Loadings (Rice) 82

Table 1b: Preliminary Sweep of Loadings (Corn) 83

Table 1c: Preliminary Sweep of Loadings (Potato) 84

Table 2a: Delayed Robbins-Monro Results (Rice) 86

Table 2b: Delayed Robbins-Monro Results (Corn) 87

Table 2c: Delayed Robbins-Monro Results (Potato) 88

Table 3: Particle Size Analysis 89

Table 4: Lower Explosive Limits 91

LIST OF FIGURES

Theoretical prediction of the temperature profile of a flame front.	6
Model of a hurning cloud (Mitsui and Tanaka).	9
Plot of the extinction coefficient versus a particle size parameter.	15
The modified Hartmann chamher.	18
The USG MRL 20 litre spherical chamber.	24
A chemical ignition source.	26
Electrical control circuit for the USG MRL 20 litre chamher.	28
Dispersion system used in the USG MRL 20 litre chamher.	31
The multi-heam light attenuation probe.	33
Electrical circuit for the multi-heam light attenuation prohe.	35
Calihration curve typical of LED/PT light attenuation systems. (C. Martin)	38
Sweep of various loadings of corn starch to determine the criteria for an explosion.	41
Typical traces of the pressure signal versus time for hoth an explosion and a non-explosion as well as that for a single igniter alone.	43
Trace showing the selection of an initial guess of the L.E.L. loading.	45
Sweep of loadings for rice starch showing hoth the pressure ratio and the rate ratio.	51
Sweep of loadings for rice starch showing the product of the pressure ratio and the rate ratio.	52

LIST OF FIGURES
(continued)

Sweep of loadings for corn starch showing both the pressure ratio and the rate ratio. 54

Sweep of loadings for corn starch showing the product of the pressure ratio and the rate ratio. 55

Sweep of loadings for potato starch showing both the pressure ratio and the rate ratio. 57

Sweep of loadings for potato starch showing the product of the pressure ratio and the rate ratio. 58

Plot of the delayed Robbins-Monro results for rice starch. 59

Plot of the delayed Robbins-Monro results for corn starch. 61

Plot of the delayed Robbins-Monro results for potato starch. 63

Typical trace of the light attenuation signals versus time. 67

Plot of L.E.L. vs. particle size using the multi-beam light attenuation probe (with shutters). 72

Plot of L.E.L. vs. particle size using the external probe (without shutters). 74

Plot of L.E.L. vs. [particle size]$^{-1}$ using the multi-beam light attenuation probe (with shutters). 76

Plot of L.E.L. vs. [particle size]$^{-1}$ using the external probe (without shutters). 78

INTRODUCTION

Dust explosions in grain processing and handling facilities are responsible for between 5 to 15 deaths each year. A series of grain elevator explosions which occurred in December 1977 and January 1978 resulted in $100 million in property damages. According to a study by Kameyama, et. al.[1], a comparison of fatalities which occurred during 1958 to 1968 with those during 1968 to 1978, indicates an increase in deaths.

In grain elevators, dust shed by grain in transport accumulates along conveyors, in ducts, and on the floor. If this dust is put into suspension and ignited by, say, a spark from a conveyor motor, an explosion may occur. However, this would be an isolated cloud producing little damage. It has been shown that the major damage occurs when this explosion shakes loose larger accumulations of dust which produce a secondary explosion capable of causing severe damage to the elevator.[2,3]

As will be brought out more clearly later, the ability of a suspension of dust particles (dust cloud) to produce an explosion (a propagating flame) depends upon the dust concentration of that cloud. If the concentration is large enough, a flame can propagate through the cloud. However if the concentration is too small, the propagation will eventually cease. This minimum concentration of dust which is capable of sustaining a propagating flame is known as the lower explosive limit.

The lower explosive limit (L.E.L.) is particular to a given dust and relates to the potential hazard of that dust. Clearly, the lower explosive limit is useful in setting intelligent safety standards concerning the levels of dust that are allowed to accumulate in grain handling facilities.

A vast majority of the present L.E.L. data available has been obtained using the Hartmann bomb. Critics claim however that the Hartmann bomb is not the best possible apparatus for measuring dust explosibility. Hertzberg, et. al.[4] have shown that the size of the ignition source has a marked influence upon the L.E.L. They report that an adequate source should produce an energy in the range of hundreds of Joules.

Other concerns of the Hartmann apparatus include the dispersion system. It has been observed, Eggleston, et. al.[5], that the Hartmann apparatus produces non-uniform dust distributions, leading to inaccuracy of the true concentration measurement. In general, the density of dust is greater along the walls of the vessel (away from the point of ignition). In addition, variations in the dispersing pressure produced variations in the density near the ignition point. These problems are also pointed out by Cashdollar et. al.[6].

Since these observations concerning the Hartmann bomb were made, many researchers have designed alternative test apparatus, with primary focus given to such parameters as the size and shape of the vessel, the dispersion system, and the ignition source. Specific oriteria for making lower explosive limit measurements have been suggested by Eckhoff[7].

First, the development of a suitable dust cloud must be perfected. Although it would be impossible to produce a perfect cloud at rest in space, a quiescent cloud, settling slowly due to gravity alone in a Stokes sense is considered to be best.

Consideration must be given to the spatial as well as temporal distribution of the local dust concentration. Along this vein, Eckhoff discusses the "scale of scrutiny". The scale of scrutiny takes into account the size of the entire cloud, the size of the ignition source, and the scale of the variations of dust concentration throughout the entire cloud. In essence, the size of the ignition source should be larger than the average size of significant density variations yet be small with respect to the cloud as a whole.

Also to be considered, is how well the dust is dispersed. The dispersion system should not allow the formation of agglomerates nor should it significantly change the particle size distribution.

Secondly, the determination of whether an explosion has or has not occured must be subjectively defined. Past researchers have employed two methods. One method relies upon the maximum pressure developed during an explosion. If the maximum pressure exceeds a set limit, then an explosion is said to have occurred. Similarly, the other method sets a limit on the diameter of the flame front produced. However, since past work has relied on direct observation to determine the flame size, this method would be either inaccurate or technically unfeasible. In the studies conducted by Hertzberg, et. al., the ratio of the peak pressure

obtained to the peak pressure of the ignition source alone was used as a criteria for ascertaining whether an explosion had or had not occurred. In their report, they took the ratio of 3.0 to be a conservative cut-off point. For the present work, involving the determination of the L.E.L. of three agricultural starches, we have considered both the peak pressure as well as the peak rate of pressure rise. In an effort to maintain a conservative stance, we have adopted a cut-off point based upon the product of the peak pressure ratio and the peak rate ratio. Finally, no L.E.L. study would be complete without accurate concentration measurements. Researchers in past studies have either determined the concentration indirectly by assuming a uniform dispersion of the dust into the chamber and thus dividing the mass of loaded dust by the chamber volume (the "nominal" concentration), or directly by removing a sample of the cloud near the ignition source. More recently, techniques based on the attenuation of light through the cloud have proven to be advantageous since in addition to being both direct and in situ measurements, they also provide information about the temporal variation of the concentration.[8]

THEORY

Any study of a lower explosive limit requires an understanding of the physical processes involved in an explosion. Several theoretical models have been developed, some more complex than others, to explain how dust explosions behave. Important parameters which explosion theories attempt to address are the minimum ignition temperature, the L.E.L., and the rate of pressure rise.

The rapid burning of a collection of dust particles is the result of four processes involving chemical reactions and heat transfer mechanisms which occur in a cyclical fashion. First, heat is supplied to the surface of a dust particle which causes an increase in its temperature. Second, oxidation occurs on the surface which allows for further temperature increase or depending upon the material, inflammable gases may be produced. Third, the incresase in temperature along with mixing of gases given off with the ambient air leads to accelerated reaction and the production of flame. Fourth, heat produced by the flame is transferred via radiative and convective means to neighboring particles.

Theoretical analysis of the structure of the flame front, provided by Toong[9], indicates that temperature gradients such as those shown in Fig. 1 occur during ignition. If ignition is successful, the temperature profile t_1 will propagate to the right and consume more reactants. However, if ignition is unsuccessful, the temperature profile will resemble t_2. It will

FIGURE 1

Theoretical prediction of the temperature profile of a flame front. Curve t_1 represents a propagating flame front. Curve t_2 represents the case of decaying propagation. (Toong, 1985)

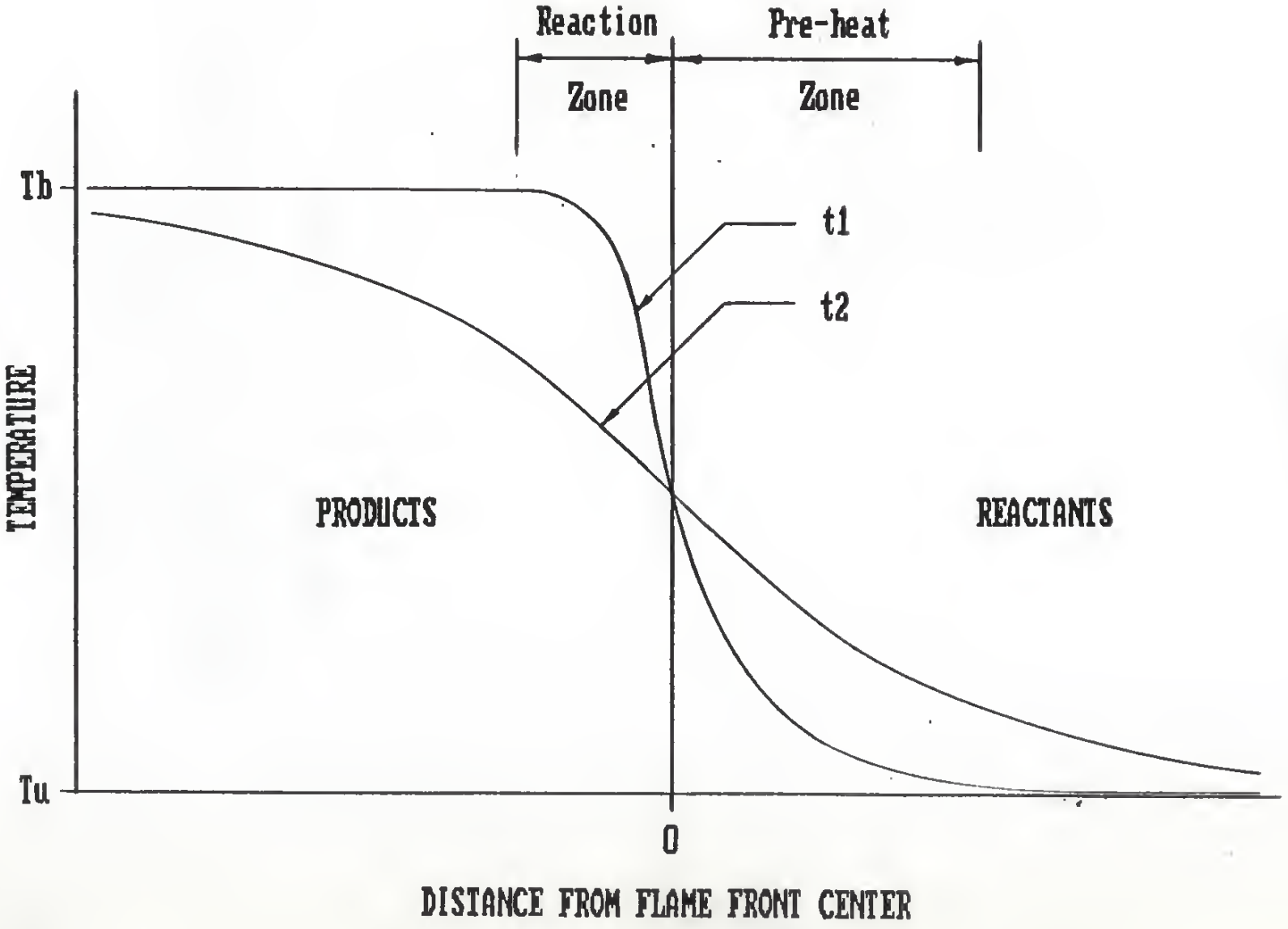
Reaction
Zone
Pre-heat
Zone
Tb
Tu
t1
t2
TEMPERATURE
PRODUCTS
REACTANTS
0
DISTANCE FROM FLAME FRONT CENTER

spread out and eventually the propagation will cease.

The ignition of a dust particle, as noted before, depends upon the chemical properties of the material. Using a simple model, Mitsui and Tanaka[10] determined the ignition temperature by equating the rate of heat generated by a dust cloud to the rate of heat transferred away from the cloud due to both radiation and convection. In their paper they state that the agreement between the theory and the experimental results of both Hartmann and Nagy (1944)[11] and Cassel and Liebmann (1959)[12] is quite satisfactory. Using a model of a uniform dust cloud whose particles are spaced apart a distance L, centered about the first burning particle, n = 1, as shown in Fig. 2, Mitsui and Tanaka are able to determine a condition under which burning will or will not propagate. By comparing the time required to raise the temperature of the second particle, T_d, to the ignition temperature, T_o, with the time for complete combustion of the first particle, it is shown that if the time of combustion of the first particle is less than that required to raise T_d of the second particle to T_o, then propagation will cease. This also allows for a prediction of the lower explosive limit which would occur when the time for complete combustion of the first particle is exactly equal to the time to raise the temperature of the second particle to the ignition temperature. Application of this time constraint leads to a prediction of the particle spacing L_o associated with the L.E.L. and hence a concentration.

Problems with this model include assumptions that the peak pressure and maximum rate of pressure rise occur at the same

FIGURE 2

Model of burning particles where: R_b = radius of the flame front, D_p = particle diameter, and T_f = temperature near the flame front. (Mitsui and Tanaka, 1973)

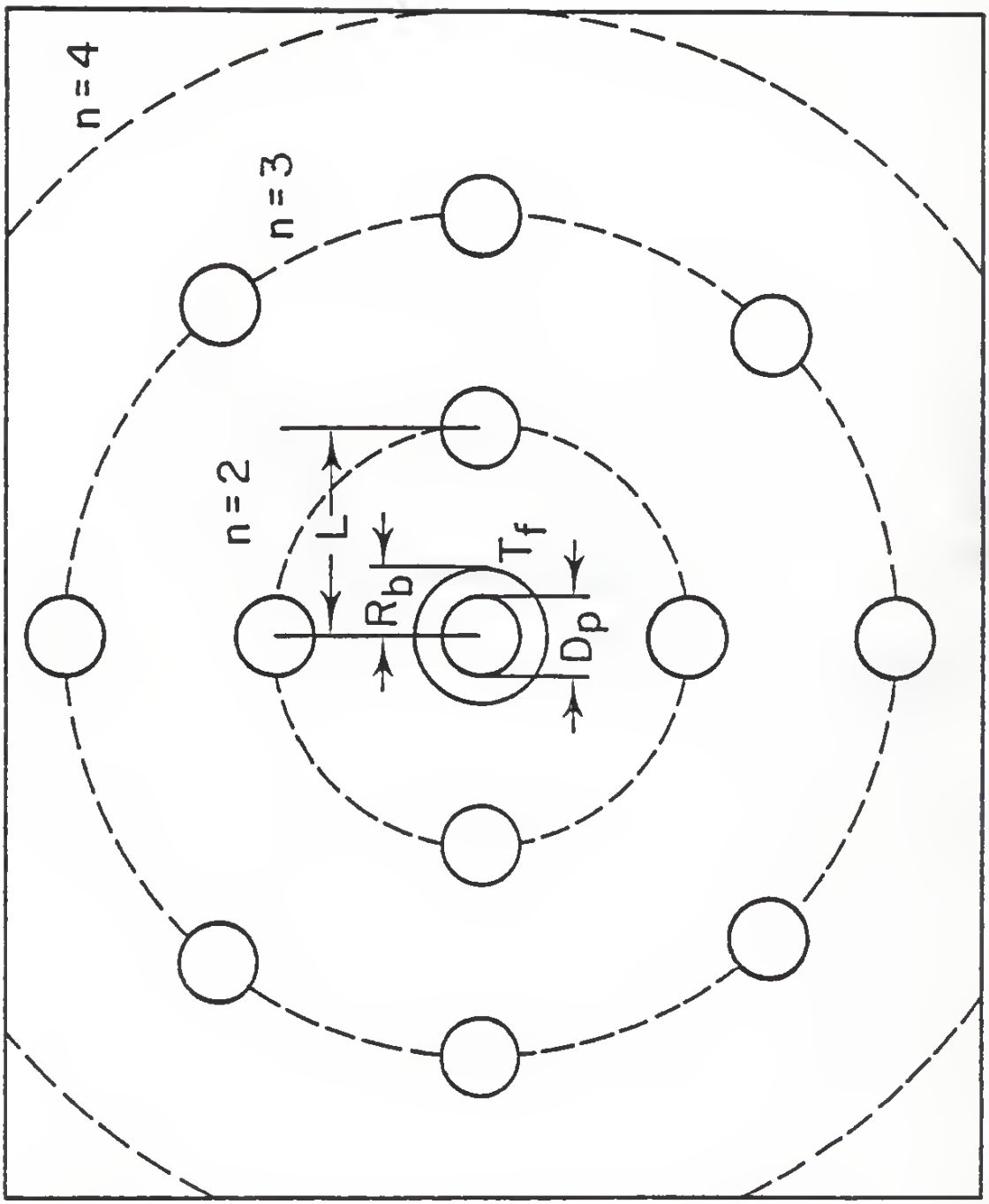
n=4
n=3
n=2
L
R_b
T_f
D_p

time, and neglect of the compression of unburnt gas ahead of the flame front. Other models of pressure development of gas explosions include those of Nagy, *et. al.*[13], and Bradley and Mitcheson[14]. Although these models have agreed reasonably well with experimental results, they are none-the-less derived for gaseous explosions and assume that the flame front is thin. A more-realistic extension to dust explosions would need to assume a flame front of finite thickness.

CONCENTRATION MEASUREMENT

The concentration of a suspended dust cloud is related to the transmission of light through the cloud by the Bougert-Beer-Lambert law.[4]

$$I = I_o \exp(-Q A n L) \qquad (1)$$

where: Q = extinction coefficient

A = cross sectional area of a particle

L = path length of the beam

n = number of particles per unit volume

I = intensity of light entering the detector

I_o = intensity of light leaving the source

The transmittance, T, is the ratio of I/I_o.

Consider a suspension with the following characteristics:

d = mean particle diameter

p = mean particle density

n = # of particles per volume

C_m = mass concentration of the cloud

We see that,

$$A = \pi r^2 = (\pi/4)d^2$$

$$C_m = mn \quad (m = \text{mean mass of a particle})$$

$$m = p*\text{volume} = p*[(4/3)\pi r^3]$$

$$= p*(\pi/6)d^3$$

so,

$$C_m = (\pi/6)pnd^3 \quad \text{or} \quad n = (6/\pi)C_m/pd^3$$

then,

$$T = \exp\{-Q[(\pi/4)d^2](6/\pi)C_mL/pd^3\}$$

$$= \exp[-Q(3/2)C_mL/pd]$$

Thus, having assumed that the particles are spherical and homogeneously dispersed,

$$C_m = (2/3)*(pd/QL)*\ln[1/T] \qquad (2)$$

The extinction coefficient, Q, includes the loss of light due to both absorbtion and scattering. The value of Q depends upon the size of the particles (d). Ideally, in the case of

laser light and a detector which receives no scattered radiation, if the particle diameter is significantly greater than the wavelength of the light, then Q asymptotically approaches the value 2.0. The variation of Q with particle size is shown in Fig. 3.

After consideration of the ratio of particle size (5 to 100 micron) to the wavelength of light to be used (900 nm), we conclude that the dusts being investigated are best described by the asymptotic region of Fig. 3, and we have chosen a value of 2.0 for the extinction coefficient.

FIGURE 3

Plot of the extinction coefficient versus a particle size parameter in the limit that n approaches one. Specifically, the x-axis is $p = \frac{2\pi d}{\lambda}(n-1)$, where d = particle diameter, λ = wavelength of the light, and n = index of refraction of the particle.[13]

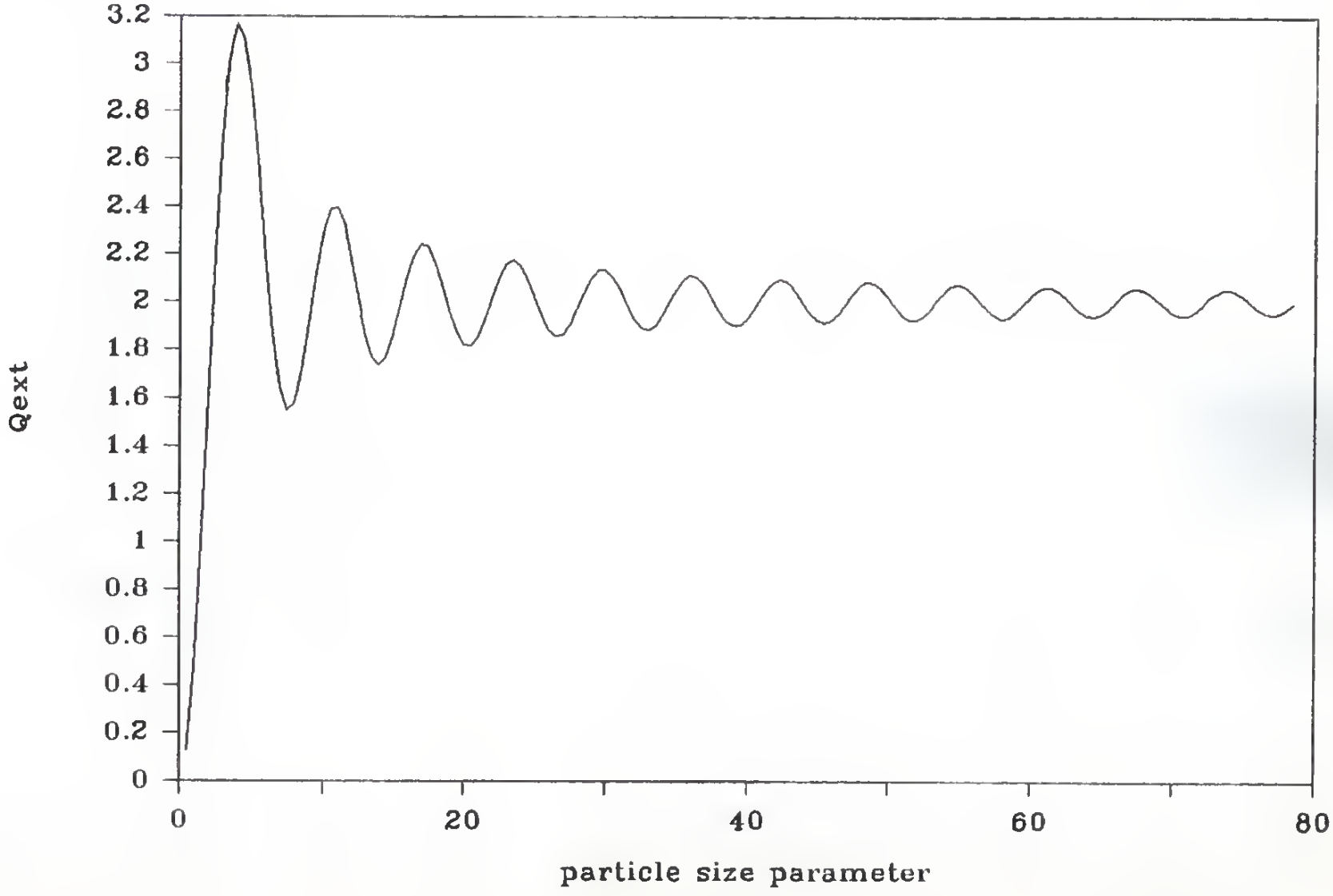
Qext
3.2
3
2.8
2.6
2.4
2.2
2
1.8
1.6
1.4
1.2
1
0.8
0.6
0.4
0.2
0
0
20
40
60
80
particle size parameter

PARTICLE SIZE MEASUREMENT

Mean particle size of the test samples was determined with a High Accuracy Particle Counter (HIAC) sensor (High Accuracy Products Corp. 1972). Test samples were dispersed in isopropyl alcohol for these measurements. A detailed discription of the HIAC method is provided by C. Martin in Appendix A.

Also, measurements were made using two other techniques for comparison of results. In one method, each sample of starch was dispersed in air in a modified Hartmann chamber. The modification of the Hartmann apparatus allows an airstream to pull dust laden air from the chamber past the HIAC sensor. See Fig. 4. In the other technique, the samples were kept in suspension in a fluid, while the attenuation of a light beam passing through the mixture was measured. By an alternative application of the Bougert-Beer-Lambert relation above, the particle size can be determined if the concentration is known.

STATISTICS OF EXPLOSION TESTING

In order to arrive at the best estimate of the threshold at which the lower explosive limit occurs based upon a finite number of trials, we have adopted the "delayed" Robbins-Monro (DRM) statistical method. In a comparative analysis with other methods, Davis[16] argues that for small and moderate sample sizes, the DRM technique is superior. A detailed discussion of this

FIGURE 4

The modified Hartmann chamber used for measurement of the particle size.

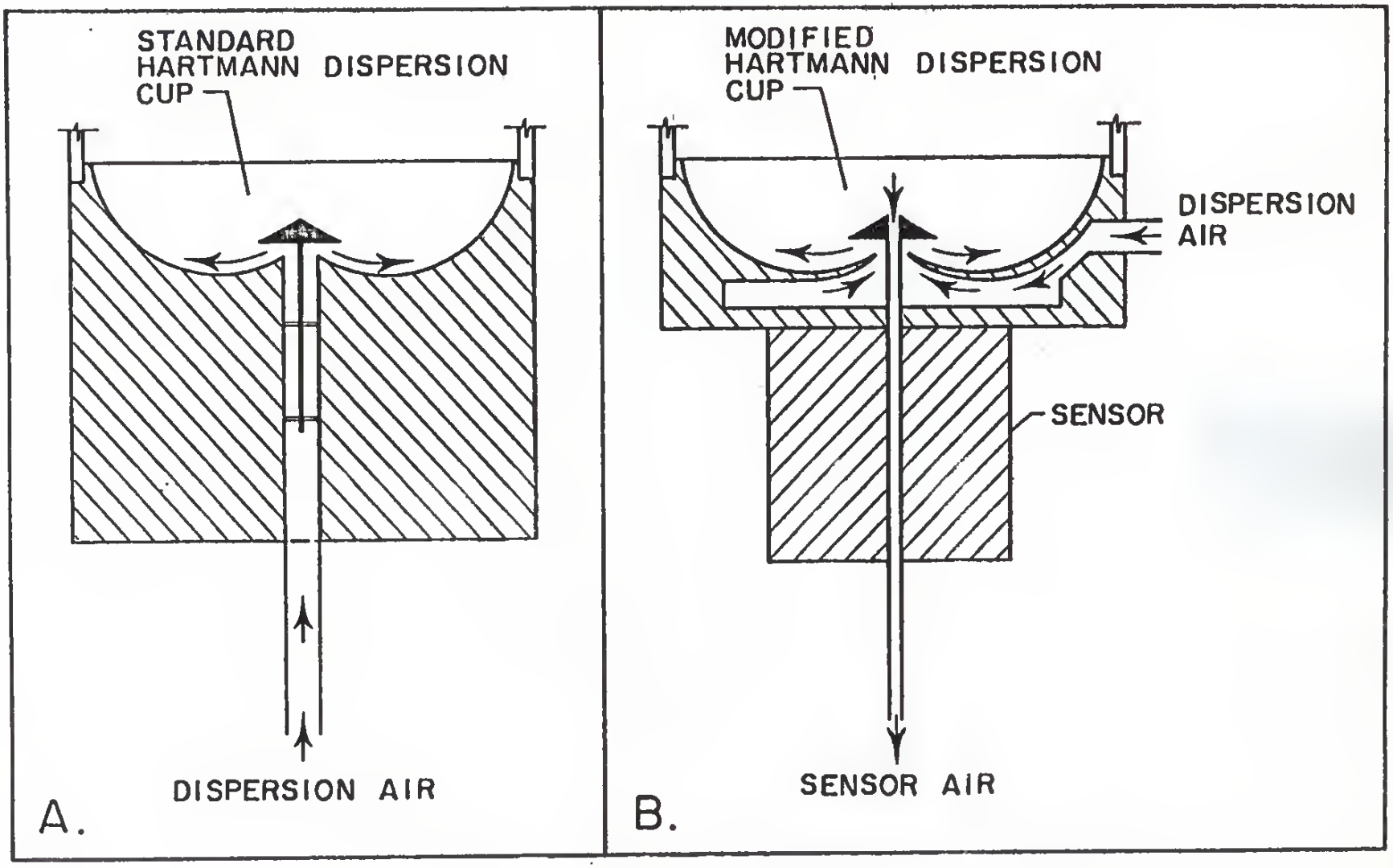
STANDARD
HARTMANN DISPERSION
CUP
DISPERSION AIR
A.
MODIFIED
HARTMANN DISPERSION
CUP
DISPERSION
AIR
SENSOR
SENSOR AIR
B.

method is provided in the literature, so only a brief outline will be provided here. According to the DRM protocol, the result of any trial is characterized as either a "go" or a "no go" (i.e. either an explosion occurs or it does not). First an initial guess of the loading (l_o) which corresponds to the L.E.L. is made. A trial at that loading is performed and based upon the result of that trial, the loading for the next trial is adjusted in the following manner:

$l = l_o \pm h$, where h is the initial step size

If the initial test is a "go", then $l = l_o - h$, $l_o - 2h$,... until the first "no go" occurs at trial $i = i^* - 1$. Likewise, if the first test is a "no go", then subsequent loadings are $l = l_o + h$, $l_o + 2h$,... until the first go occurs at trial $i^* - 1$.

Then for all trials after and including i^*, the step size is adjusted as follows:

$$l_{i \geq i^*} = l_{i-1} \pm \frac{h}{i - i^* + 2}$$

Where addition is used with a "no go", and subtraction is used with a "go".

The results of these trials can be used to produce a maximum likelihood estimate of the lower explosive limit. Each of n dust

clouds has its own unobservable lower explosive limit. It is assumed that these L.E.L.'s obey a normal probability distribution,

$$\text{Probability (L.E.L. loading} \leq \ell) = \Phi\left(\frac{\ell - \bar{\ell}}{\sigma}\right)$$

where

$$\Phi(z) = \frac{1}{\sqrt{2\pi}} \int_{-\infty}^{z} \exp(-u^2/2)\, du$$

$\bar{\ell}$ = population mean

σ = standard deviation

An appropriate likelihood function, $\mathcal{L}$, can be constructed by forming a product of the distributions of each trial.

$$\mathcal{L} = \prod_{+} \Phi(z_i) \prod_{o} [1 - \Phi(z_i)] \qquad (3)$$

where + denotes clouds which resulted in a "go", and

o denotes clouds which resulted in a "no go".

A maximum likelihood estimate is any values of $\bar{l}$ and σ which maximize equation (3). This involves solving two sets of simultaneous equations (one for $\bar{l}$, another for σ) using numerical techniques. It is simpler to maximize the logarithm of equation (3). Thus:

$$\frac{\partial}{\partial \bar{l}}[\ln \mathcal{L}] = 0 \longrightarrow \sum_{+} \alpha_i - \sum_{o} \beta_i = 0$$

$$\frac{\partial}{\partial \sigma}[\ln \mathcal{L}] = 0 \longrightarrow \sum_{+} z_i \alpha_i - \sum_{o} z_i \beta_i = 0$$

where,

$$\alpha_i = \frac{\Phi'(z_i)}{\Phi(z_i)} \qquad \beta_i = \frac{\Phi'(z_i)}{[1 - \Phi(z_i)]}$$

$$\Phi'(z_i) = \frac{d\,\Phi(z_i)}{dz_i}$$

APPARATUS

A 20 litre vessel and dispersion system has been designed and fabricated at the U.S. Grain Marketing Research Lab (Manhattan, Kansas). The vessel is made from two stainless steel end caps which are hinged for easy access. These two hemispheres are held in a steel frame and pressed together by a hydraulic piston. Outlets are provided for evacuating the chamber and for the exhaust of gases. Inlets consist of the dust dispersion system and a diametrically-opposed air inlet. A drawing of the explosion chamber and frame is shown in Fig. 5. A major safety feature of this chamber is the electrical interlock system. The interlocks prevent the user from initiating an explosion without first closing the chamber.

The ignition source consists of a 5 kJ chemical igniter. The igniters (Fig. 6) are constructed from electric matches, gelatin capsules, and FFF black powder. Assembly is done by hand in an electrically grounded environment which reduces the chance of accidental ignition by a build-up of static charge.

The entire firing sequence is controlled automatically using solid state time delayed relays (National Controls Corp. model T1K). One relay, TDR1, controls the charging of the air reservoir and is adjustable for delays of 1 to 10 seconds. The other two relays, one controlling the dispersion valve and another controlling the igniter current, can be adjusted between 0.05 and 5.0 seconds. See Fig. 7.

FIGURE 5

The U.S. Grain Marketing Research Lab's 20 litre spherical explosion chamber.

U.S. GRAIN MARKETING LAB 20-L CHAMBER

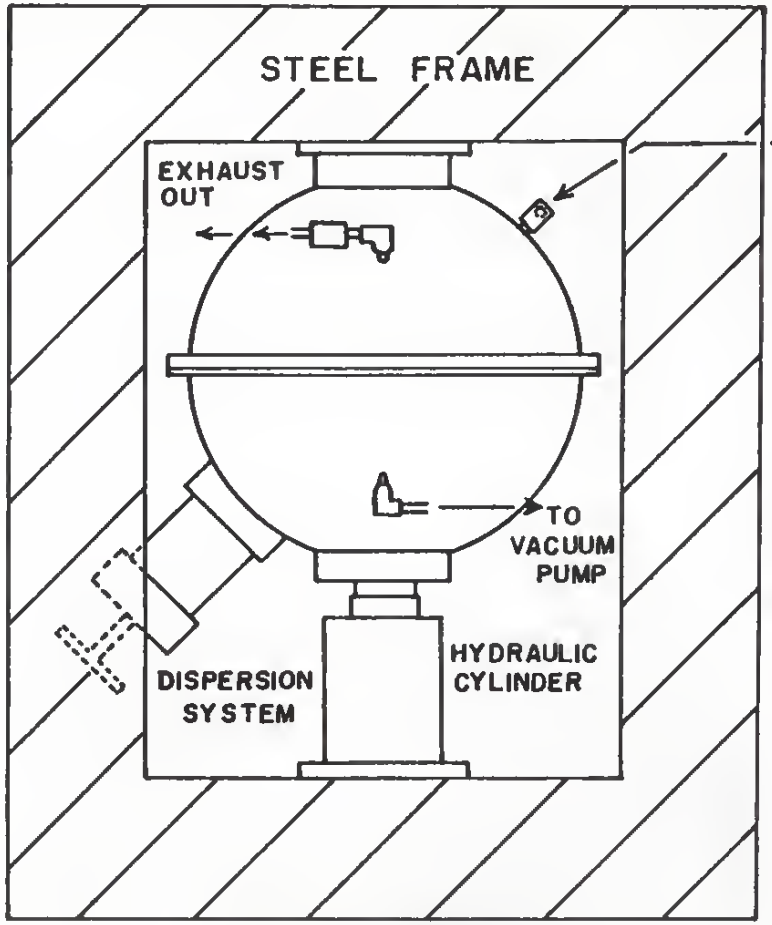

FRONT VIEW

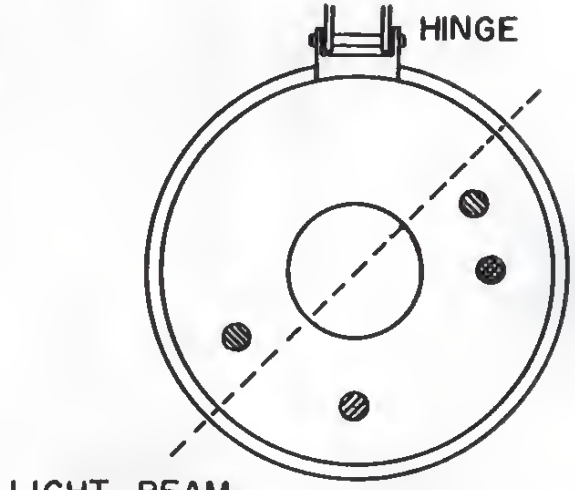

TOP VIEW

- PRESSURE TRANSDUCER
- OPPOSING AIR JET
- EXHAUST OUTLET

FIGURE 6

A high energy (5 kJ) chemical ignition source.

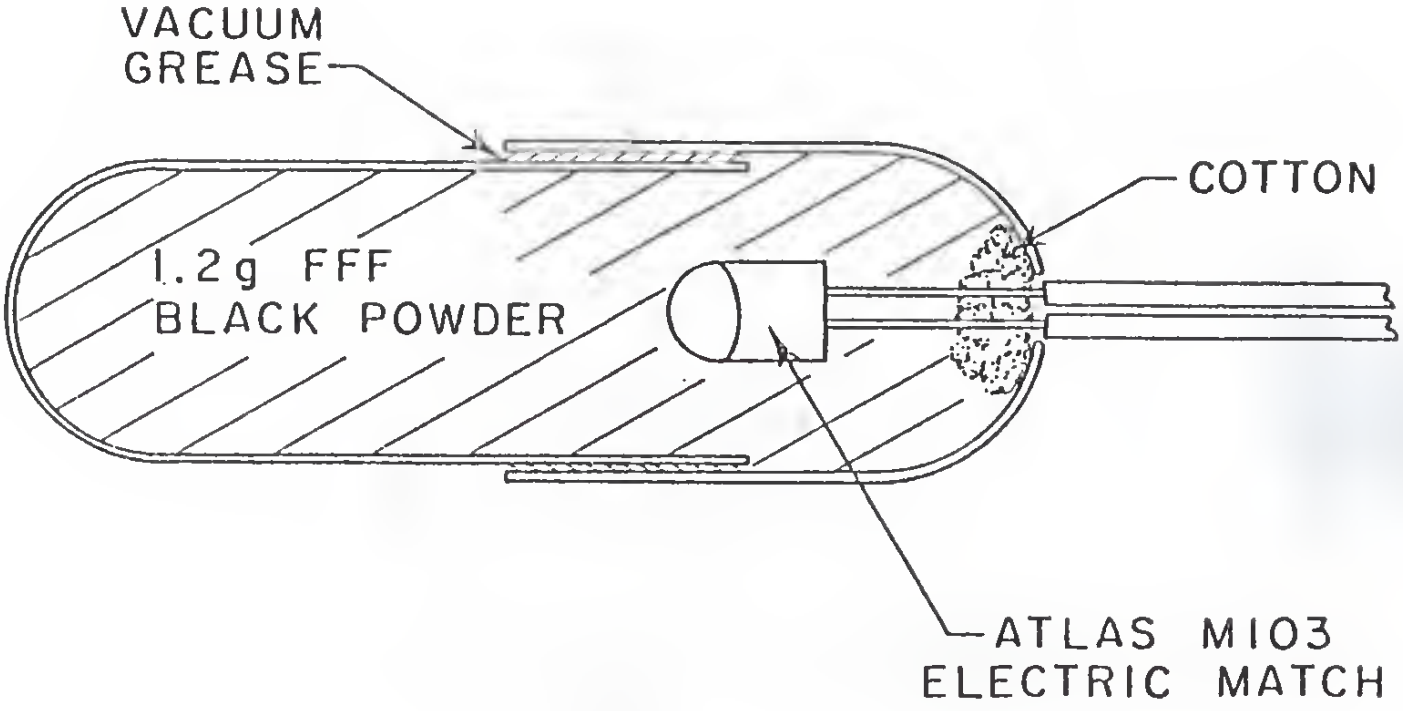
VACUUM
GREASE
COTTON
1.2g FFF
BLACK POWDER
ATLAS M103
ELECTRIC MATCH

FIGURE 7

Electrical control circuit for the USGMRL 20 litre chamber.

CONTROL CIRCUIT
FOR
USGMRL 20-L CHAMBER

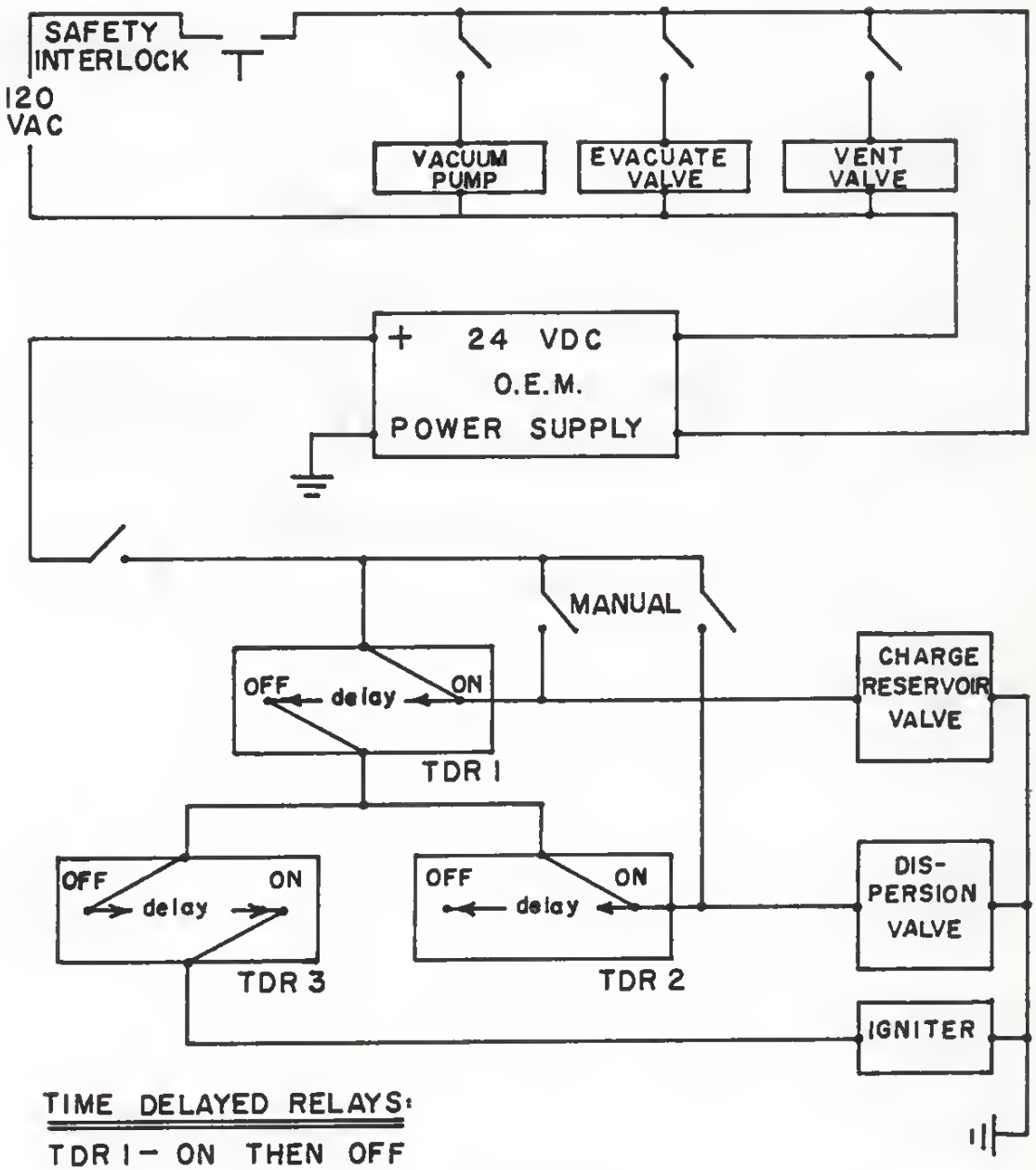

TIME DELAYED RELAYS:

TDR 1 – ON THEN OFF

TDR 2 – ON THEN OFF, DELAY = T_o

TDR 3 – OFF THEN ON, DELAY = T_d

The dispersion system developed for these studies is diagrammed in Fig. 8. Its features include a piston driven hy compressed air, a high-velocity air stream, and a plate that is perforated with small diameter holes (~3/32 inch dia.) through which the dust oloud expands into the chamber.

Pressure development prior-to and during the explosion is recorded using two Kistler model 211B4 piezoelectric transducera. The data are then transferred to a Nicolet model 4094 digital oscilloscope and stored onto 5.5 inch magnetic disks for later analysis.

To investigate the uniformity of the cloud and for concentration measurements, a multi-heam light attenuation probe was designed. The prohe is diagrammed in Fig. 9. It consists of four sets of light emitting diode (LED) and phototransistor (PT) pairs, matched at an infrared wavelength of about 900 nanometers, mounted onto a steel ring. The ring is sized so that it fits inside the homh, as close to the walls as possible. Two of the heams are located along the diameter of the ring, while the other two are along chords half a diameter away. The circuitry for the prohe is diagrammed in Fig. 10. A shutter system composed of eight covers and four solenoids, can he triggered by the ignition signal to view the attenuation at that instant without the inaccuracies induced hy dust which would normally accumulate on the lenses. The four signals derived from this device are recorded on a Nicolet 4-channel digital oscilloscope.

By varying the orientation of the ring inside the homb, we are ahle to view the attenuation of light along several different

FIGURE 8

Cut-away view of the dispersion system used in the USGMRL 20 litre chamber.

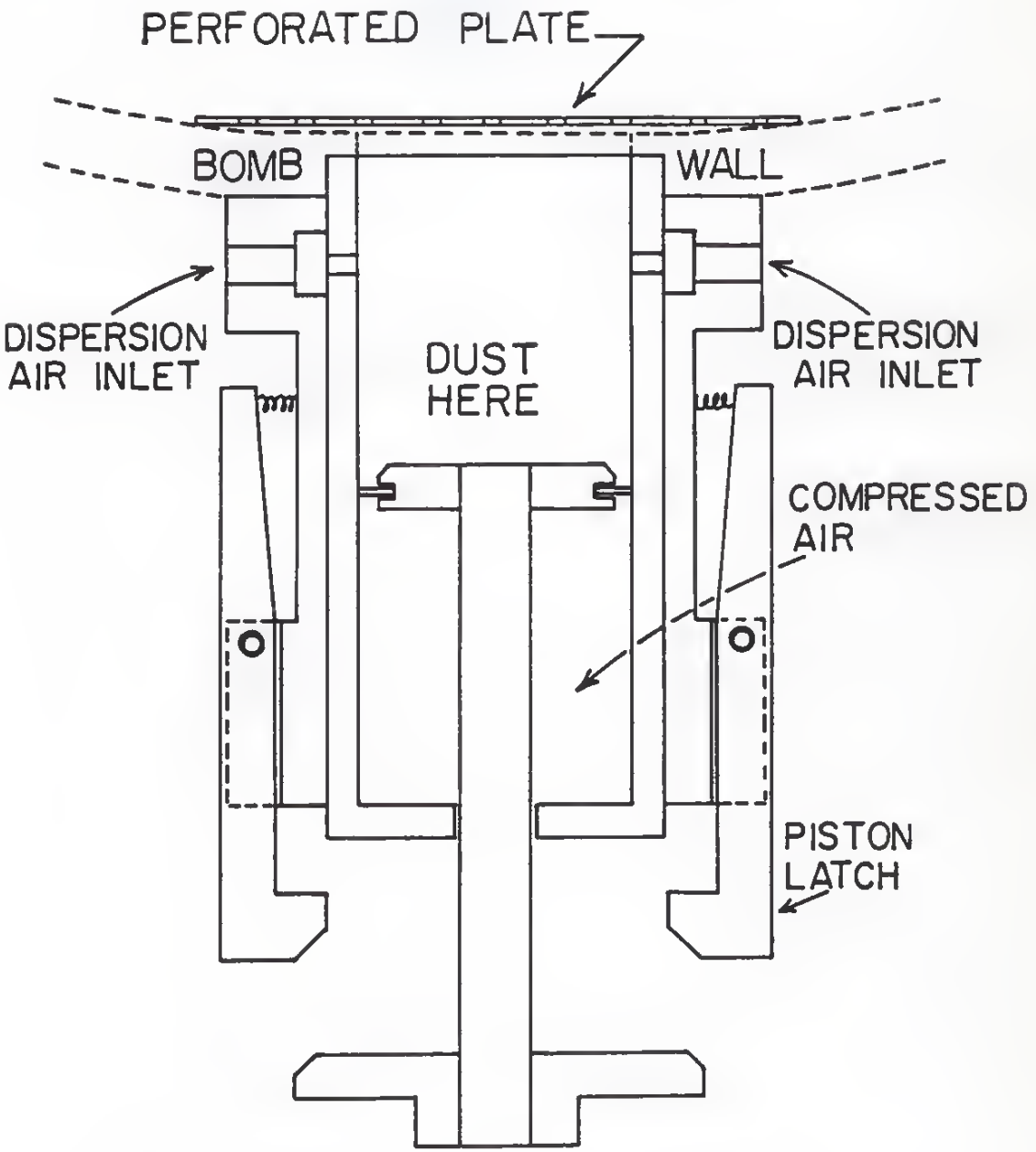

DISPERSION SYSTEM
(cross-section)

FIGURE 9

Multi-beam light attenuation probe (showing one shutter) used for characterising the uniformity of the dust cloud and for concentration measurements.

MULTI-BEAM LIGHT ATTENUATION PROBE

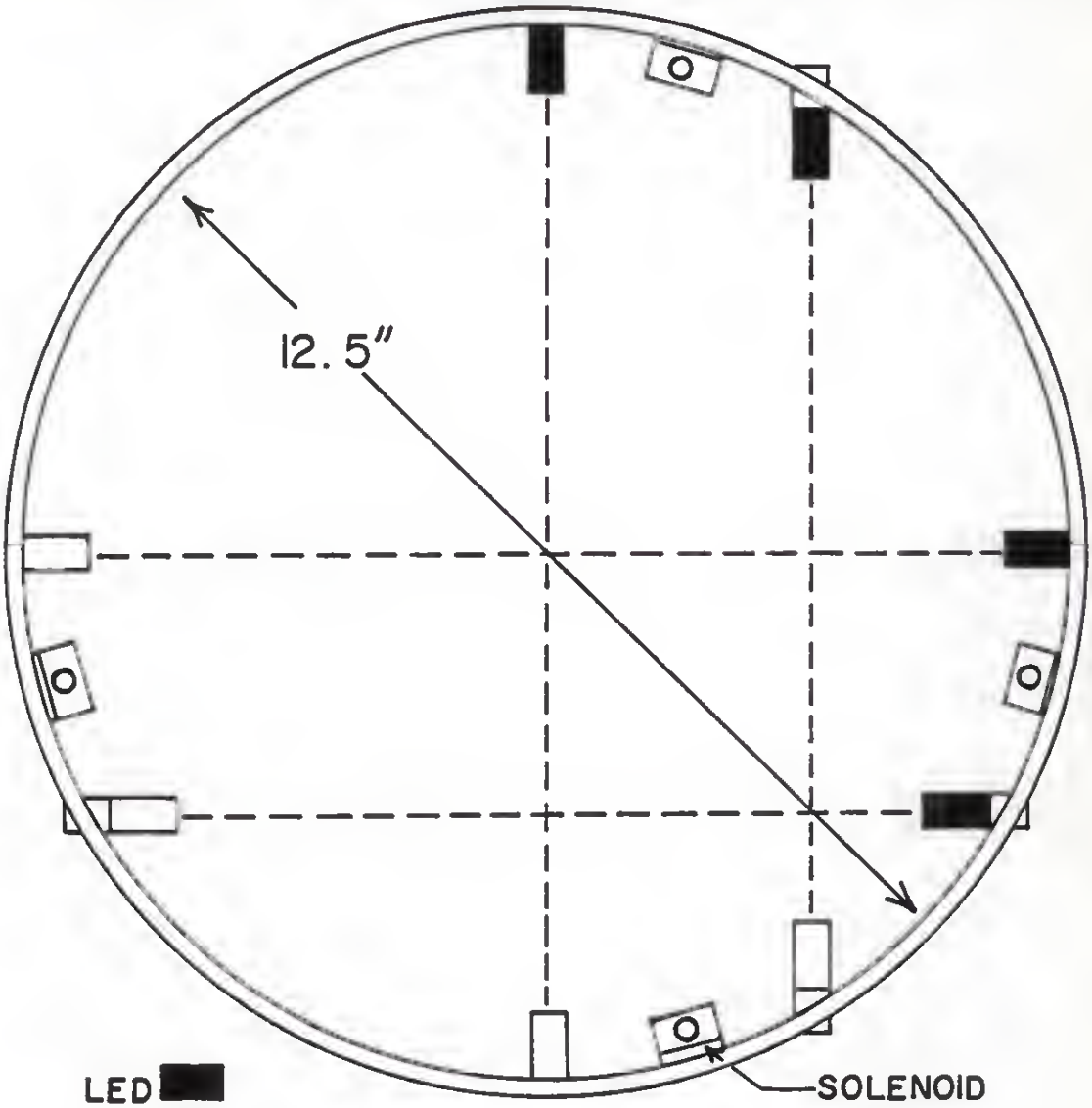

LED ■
PT □

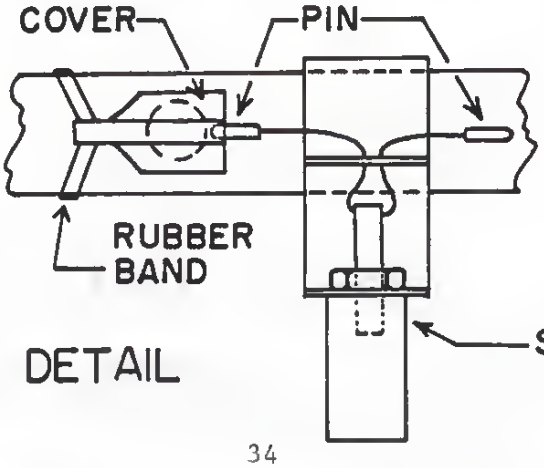

SHUTTER DETAIL

FIGURE 10

Electrical circuit for the multi-beam light attenuation probe.

MULTI-BEAM LIGHT ATTENUATION PROBE CIRCUIT DIAGRAM

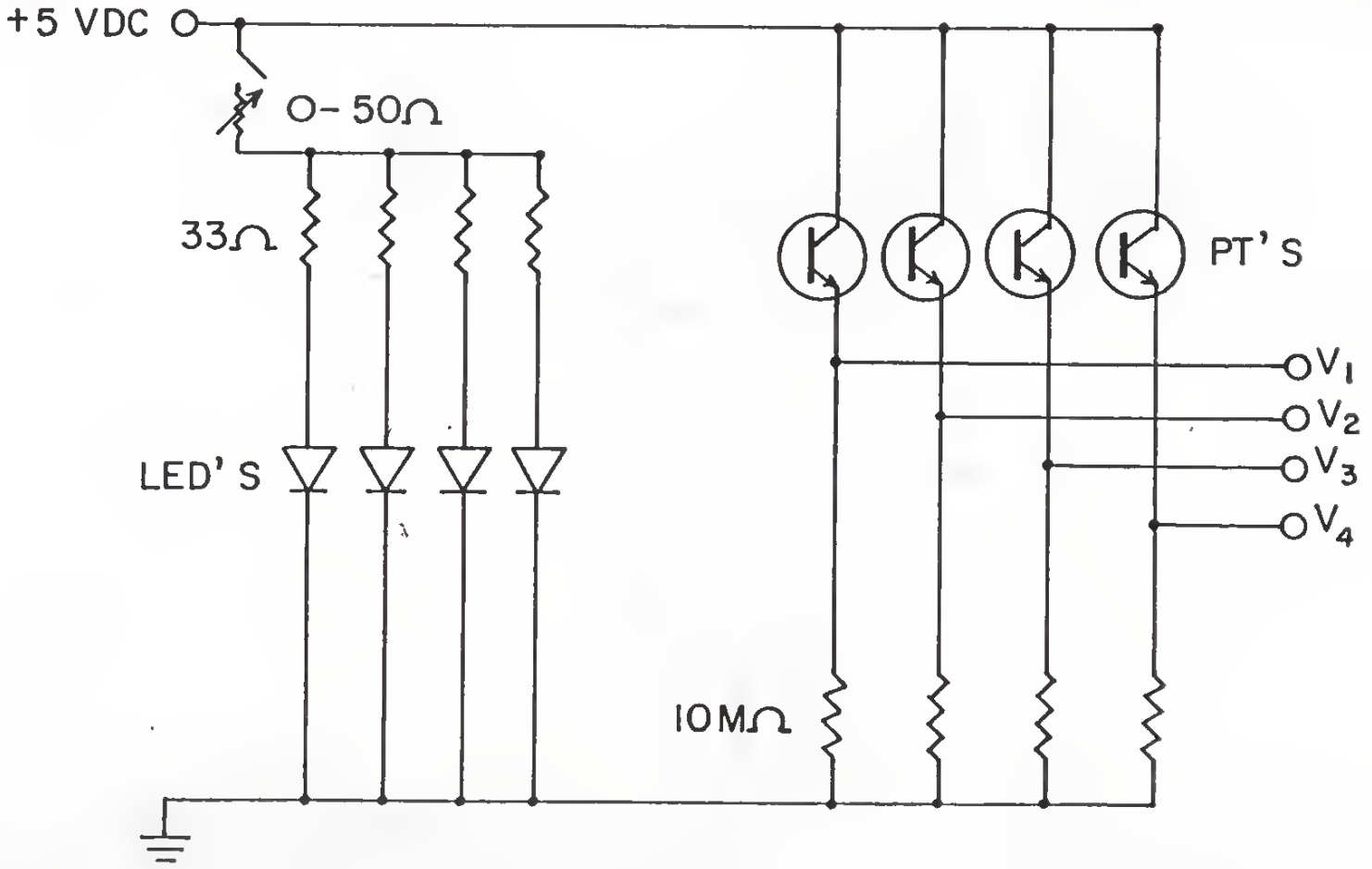

paths. Comparing the attenuation signal received from beams operating along the different axes of the chamber allows the uniformity of the cloud produced in this chamber to be characterized.

Also, by application of the Bougert-Beer-Lambert relationship (Eqn. 2), a measurement can be made of the cloud concentration along each axis. Similar LED/PT systems have been used successfully by Liebman and Conti, et. al.[17] for dust concentration measurements. The calibration of the LED/PT pairs was achieved using a set of neutral density filters whose transmittances at a given wavelength of light were known. Because the PT's are prone to saturation in various supply voltage ranges, we were unable on occasion to develop a linear response of the PT's for the entire range of transmittances. However previous work by C. Martin at USGMRL has provided a calibration curve which is applicable to such LED/PT systems (Fig. 11).

Since the four-beam probe would be damaged during an explosion test, another single beam, LED/PT pair is mounted external to the chamber. This allows the cloud concentration to be measured immediately prior to firing the igniters.

FIGURE 11

Calibration curve typical of LED/PT light attenuation systems. (C. Martin)

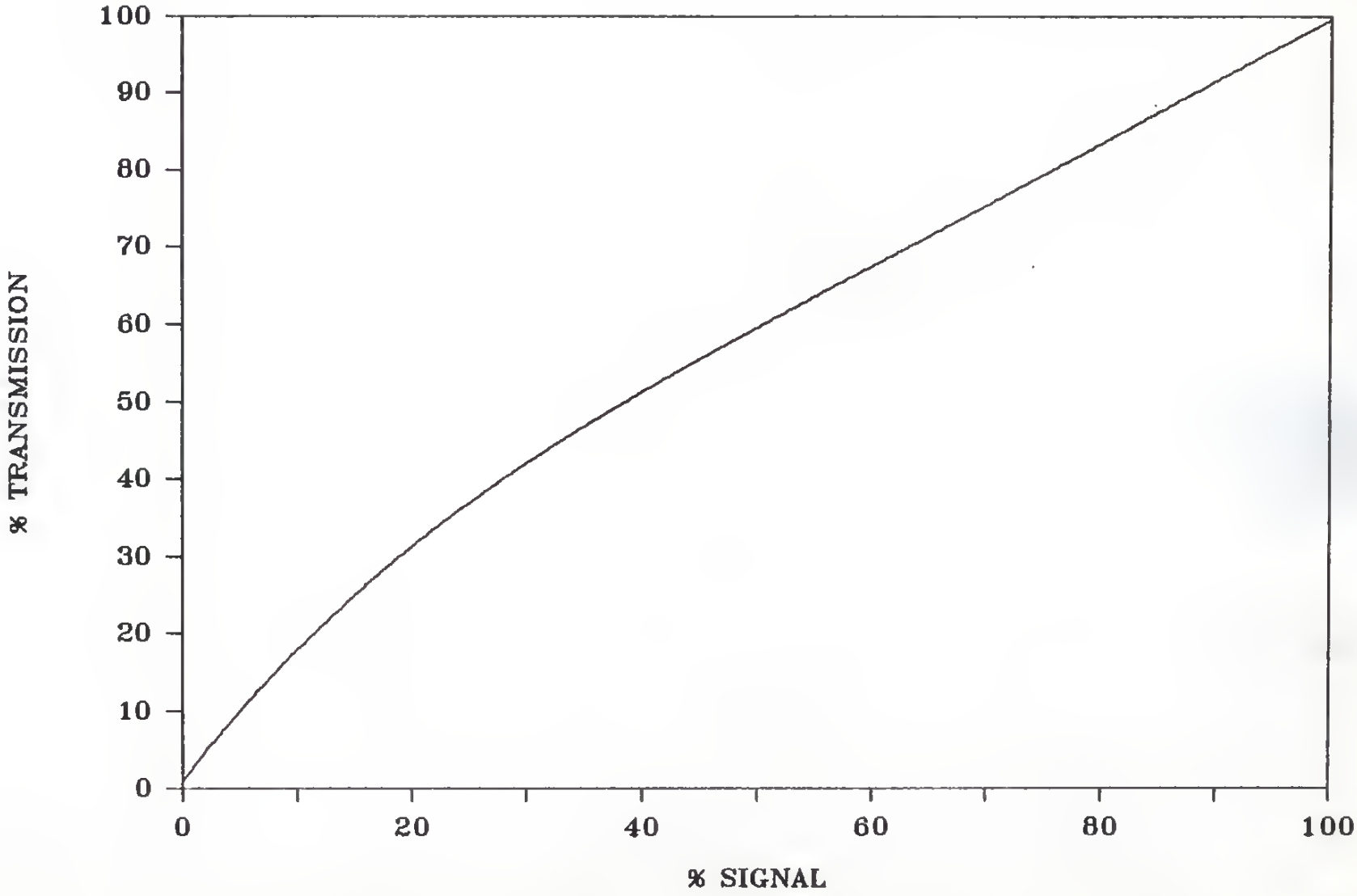
100
90
80
70
60
50
40
30
20
10
0
% TRANSMISSION
0
20
40
60
80
100
% SIGNAL

EXPERIMENT

In order to apply the "delayed" Robbins-Monro protocol a distinction must be made regarding what is and is not an explosion. Preliminary results using cornstarch revealed that the product of the peak pressure ratio and the peak rate of pressure rise ratio takes a sizeable jump over a narrow range of loadings (Fig. 12). Using this curve, and in particular the midpoint of the discontinuity shown, we have adopted the definition that an explosion has occurred if the product of the peak pressure ratio and the peak rate ratio, R, is greater than 13.0. Defined in this manner, sample traces of the pressure vs. time signal for both an explosion and a non-explosion are shown in Fig. 13. For comparison, Fig. 13 also shows the pressure vs. time signal of the ignition source alone.

The procedure for determining the L.E.L. is as follows. First, a preliminary "sweep" of trials at various loadings is made. This yields a curve such as that shown in Fig. 14, which provides both an initial guess of the L.E.L. loading and an appropriate step size to use. Next, the DRM method is applied for ten trials, to produce an estimate of the loading which corresponds to the lower explosive limit of the dust being studied. Then, once that loading is determined, several dispersions of the dust at that loading are performed and concentration measurements are made to determine the L.E.L. of the dust.

FIGURE 12

Sweep of various loadings of corn starch to determine the criteria for an explosion. The midpoint of the large jump shown corresponds to a product ratio, R = 13.

ratio
0
5
10
15
20
25
30
35
40
0
2
4
6
loading (g)
product

FIGURE 13

Typical traces of the pressure signal versus time for both an explosion and a non-explosion as well as that for a single igniter alone. The signal decay (after reaching the peak pressure) is due to the response of the quartz crystals of the transducers and does not represent the pressure at that time.

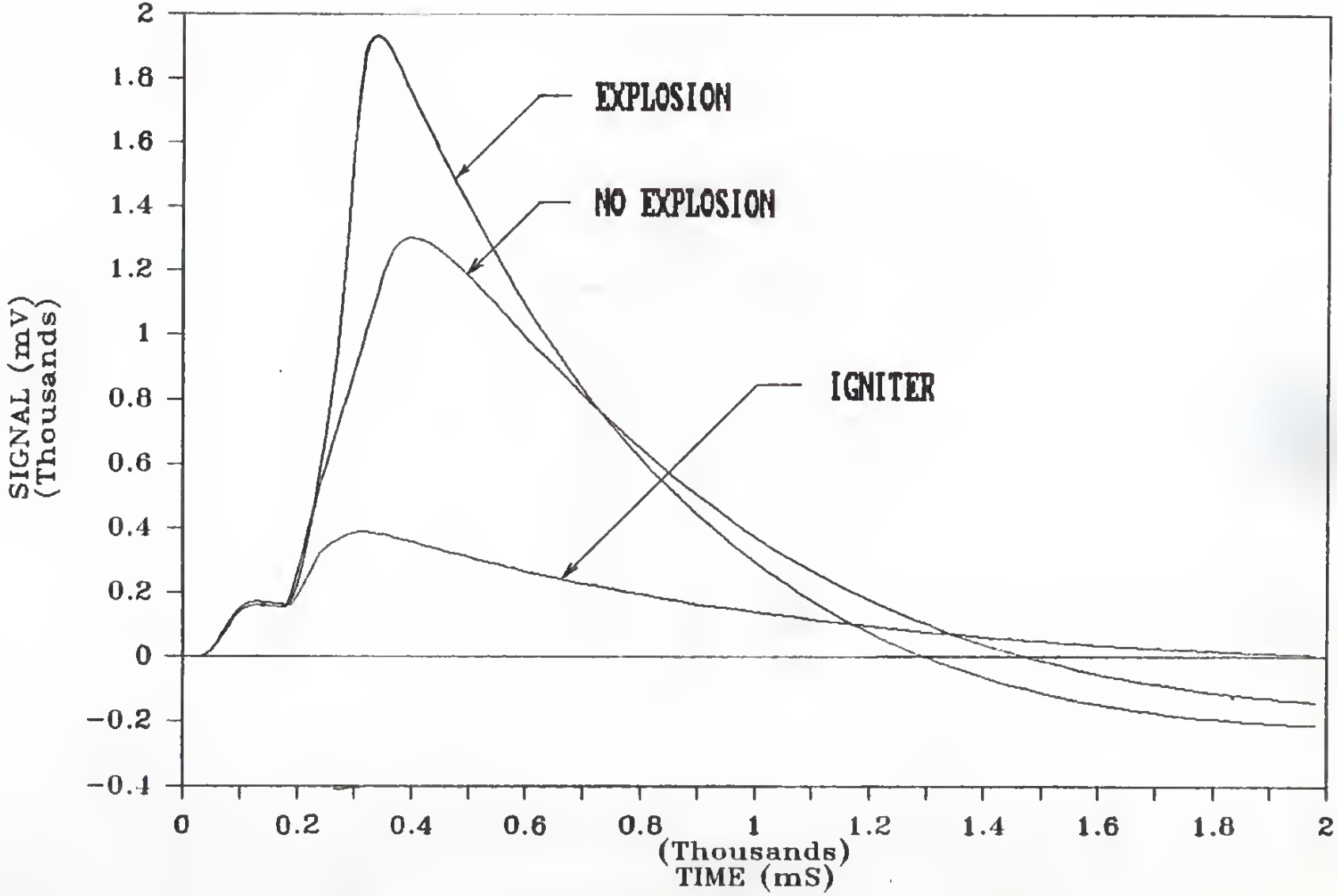
EXPLOSION
NO EXPLOSION
IGNITER
SIGNAL (mV)
(Thousands)
2
1.8
1.6
1.4
1.2
1
0.8
0.6
0.4
0.2
0
-0.2
-0.4
0
0.2
0.4
0.6
0.8
1
1.2
1.4
1.6
1.8
2
(Thousands)
TIME (mS)

FIGURE 14

Sample trace showing the selection of an initial guess of the L.E.L. loading based upon the definition of an explosion and a sweep of loadings. The horizontal line (R = 13) represents the explosion/non-explosion threshold.

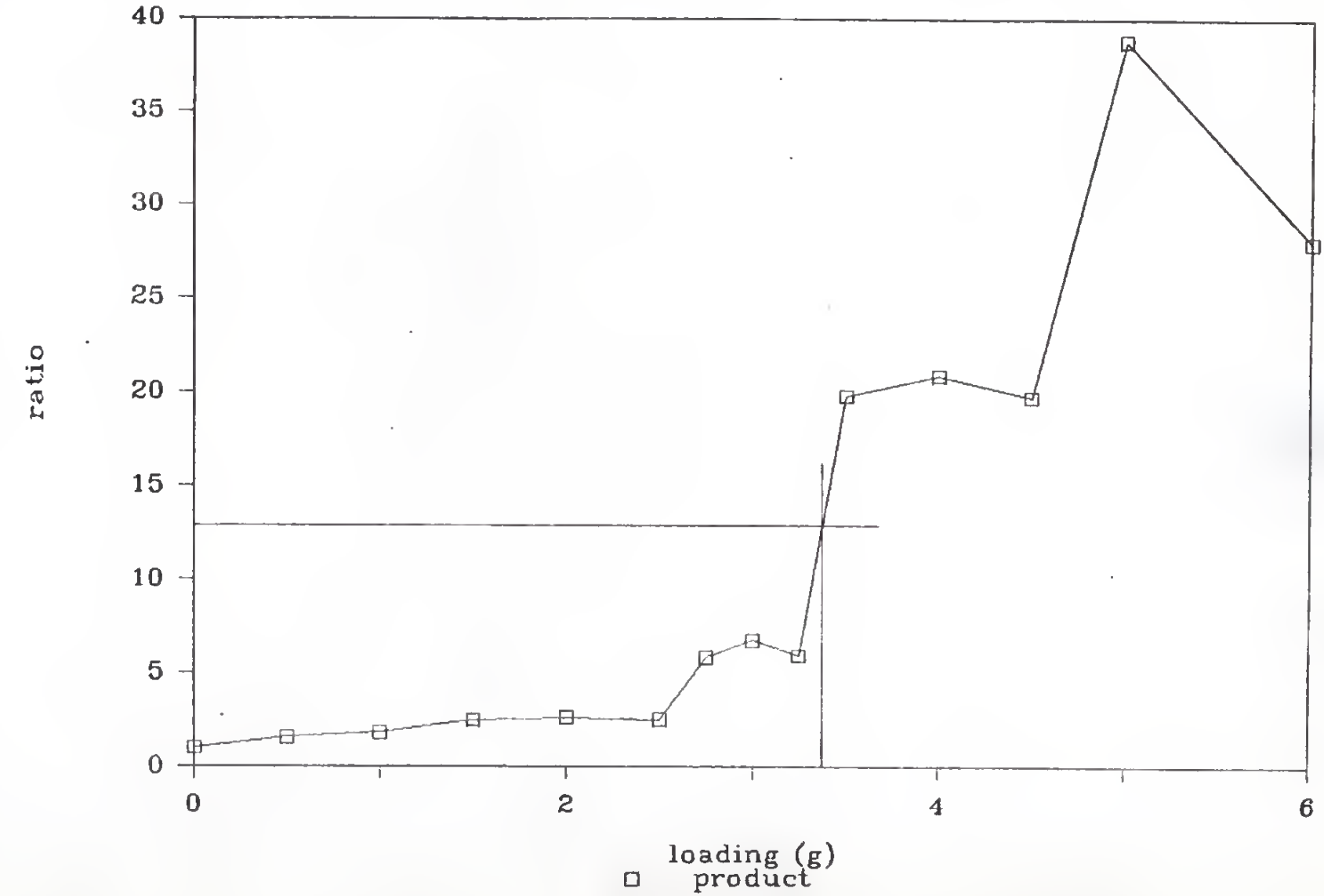
40
35
30
25
20
15
10
5
0
ratio
0
2
4
6
loading (g)
product

PROCEDURE

The procedure for exploding dusts in the 20 litre sphere is as follows, and is supplimented by a diagram of the control circuitry in Fig. 7.

Starting with the piston retracted, a dust sample is loaded into the cavity; a chemical igniter is installed; and the chamber is closed and secured. The vessel is then evacuated to a pressure such that, after having dispersed the dust, the final pressure in the vessel immediately prior to ignition is one atmosphere. Next, the firing sequence is initiated. First, TDR1 opens a solenoid valve for 10 seconds to charge the air reservoir to 300 p.s.i. Following this, TDR2 opens the dispersion valve for a time T_o = 100 ms. This carries the dust into the airstream and through the perforated plate. Finally at a time T_d = 180 ms after TDR1 finishes, TDR3 sends current to the igniter.

SAMPLE PREPARATION

Three starches were studied: rice starch, corn starch, and potato starch. Each starch sample was freeze dried and stored in a dessicator. The density was measured by determining the mass of a sample and then determining the volume which it displaced inside a helium filled chamher (Quantachrome Corp. Stereopycnometer, Model Spy 2-F6). The moisture content was determined by measuring the mass change which occurred when a 3 g. sample of each dust was dried in an oven at 103 degrees Celsius for three hours.[18]

RESULTS AND DISCUSSION

Results of the initial sweep of loadings for each starch are listed in Tables 1a, 1h, and 1c. Graphical displays of the initial sweep of loadings can he found in Figs. 15, 16, and 17. Similarly, results of the delayed Rohbins-Monro trials are listed in Tahles 2a, 2h, and 2c. Graphical displays of the delayed Rohhins-Monro results can be found in Figs. 18, 19, and 20.

Time did not allow the construction of an appropriate computer algorithm capable of determining the maximum likelihood estimates of each starch's L.E.L. loading. The values which are quoted in Tables 2a, 2b, and 2c have heen estimated hy assuming that the width of the overlap (i.e. $l_a - l_h$, where an explosion

had occurred at the loading l_a and no explosion had occurred at the loading l_b, such that $l_a < l_b$) is representative of the standard deviation, and that the L.E.L. loading can be approximated as:

$$\text{L.E.L. loading} = \frac{l_a + l_b}{2}$$

A. Error

Pressure measurements are precise to 0.35 bar, and time intervals are precise to about 0.5 ms. The error in measuring the mass of the loaded dust is about 5 mg. The voltages produced by the phototransistors could be measured to within 5 mV and the error in determining the transmittance was less than 1%.

FIGURE 15a

Sweep of loadings for rice starch showing both the pressure ratio and the rate ratio.

FIGURE 15b

Sweep of loadings for rice starch showing the product of the pressure ratio and the rate ratio.

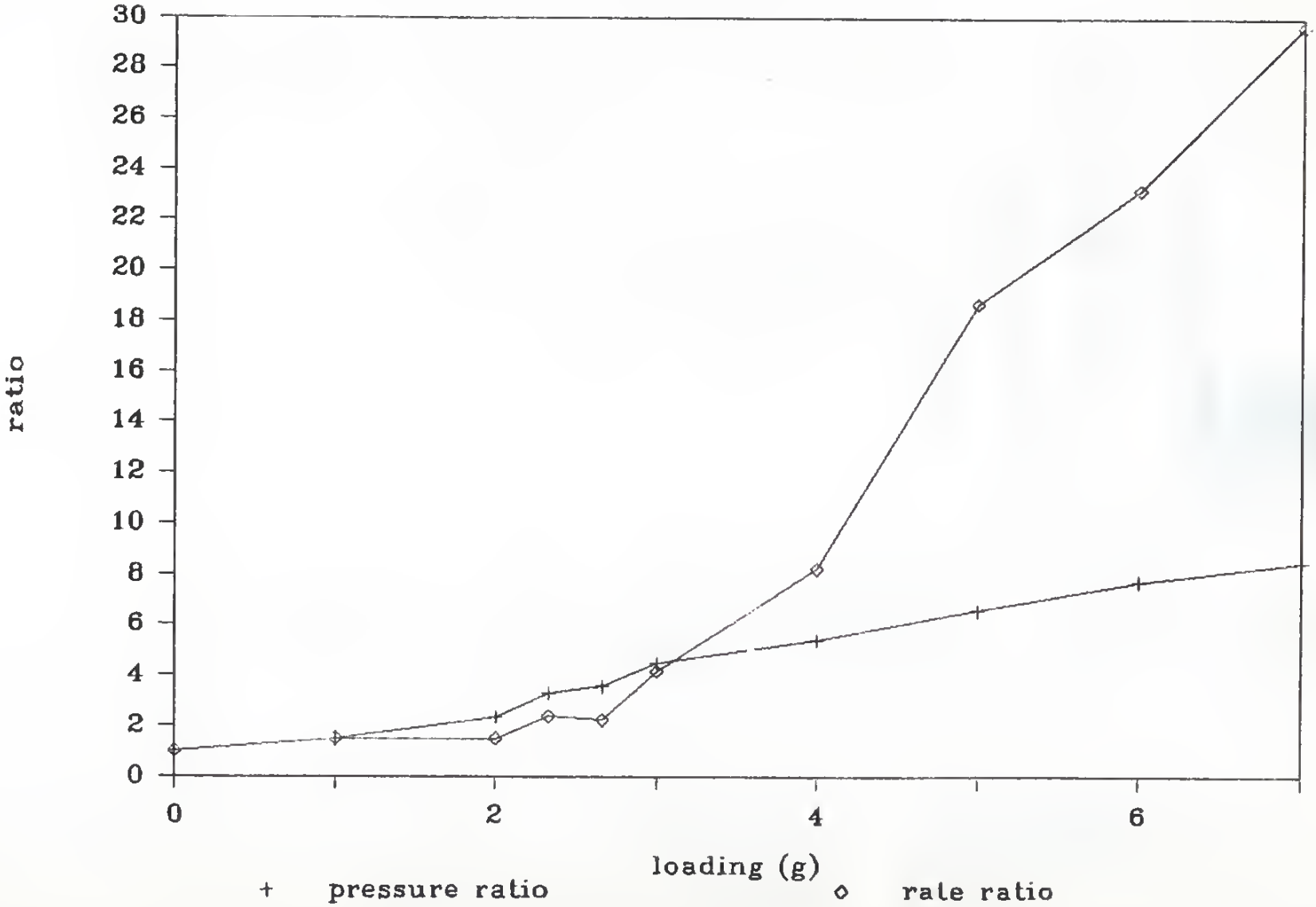
30
28
26
24
22
20
18
16
14
12
10
8
6
4
2
0
ratio
0
2
4
6
loading (g)
+ pressure ratio
◇ rate ratio

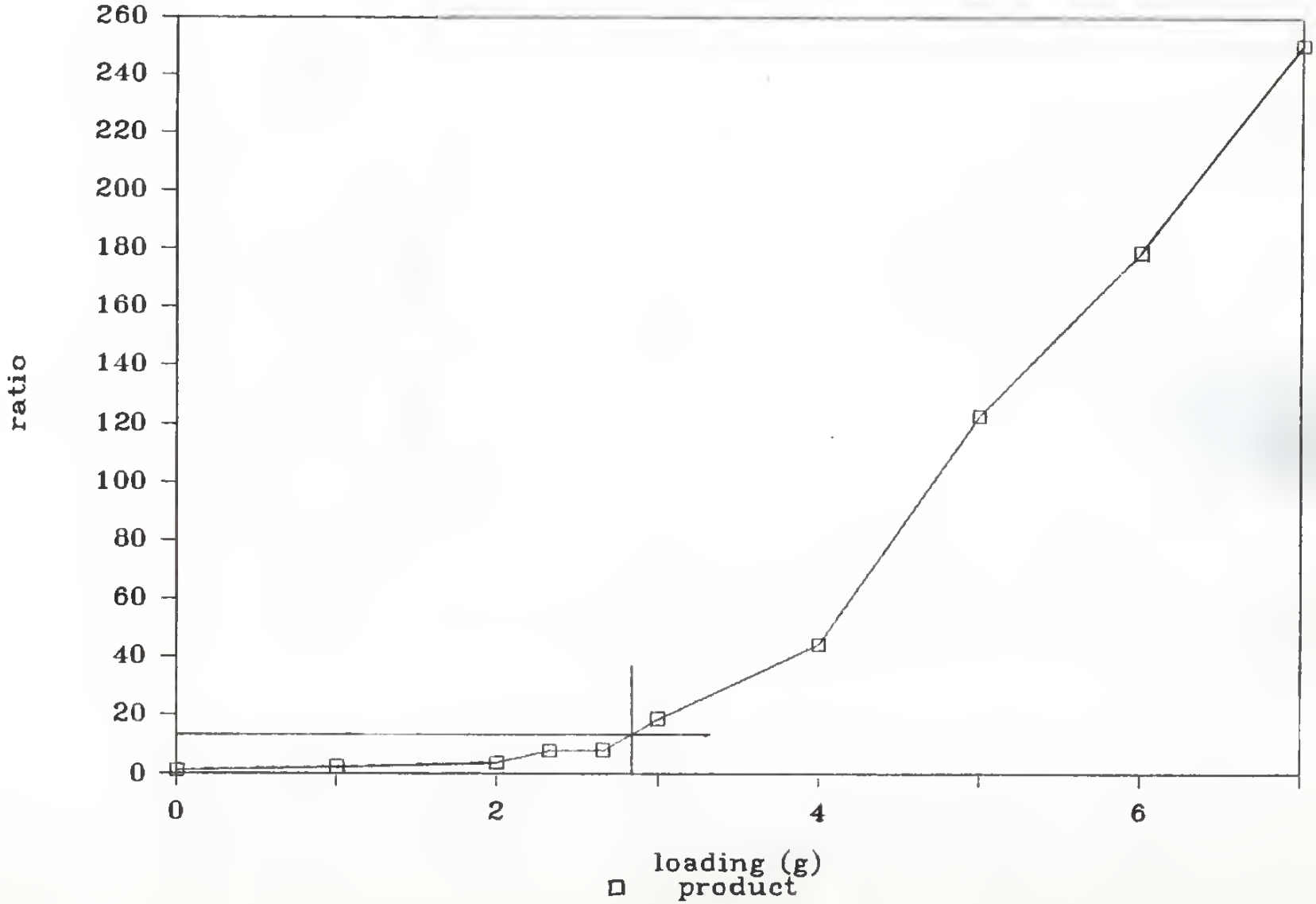
260
240
220
200
180
160
140
120
100
80
60
40
20
0
ratio
0
2
4
6
loading (g)
product

FIGURE 16a

Sweep of loadings for corn starch showing both the pressure ratio and the rate ratio.

FIGURE 16b

Sweep of loadings for corn starch showing the product of the pressure ratio and the rate ratio.

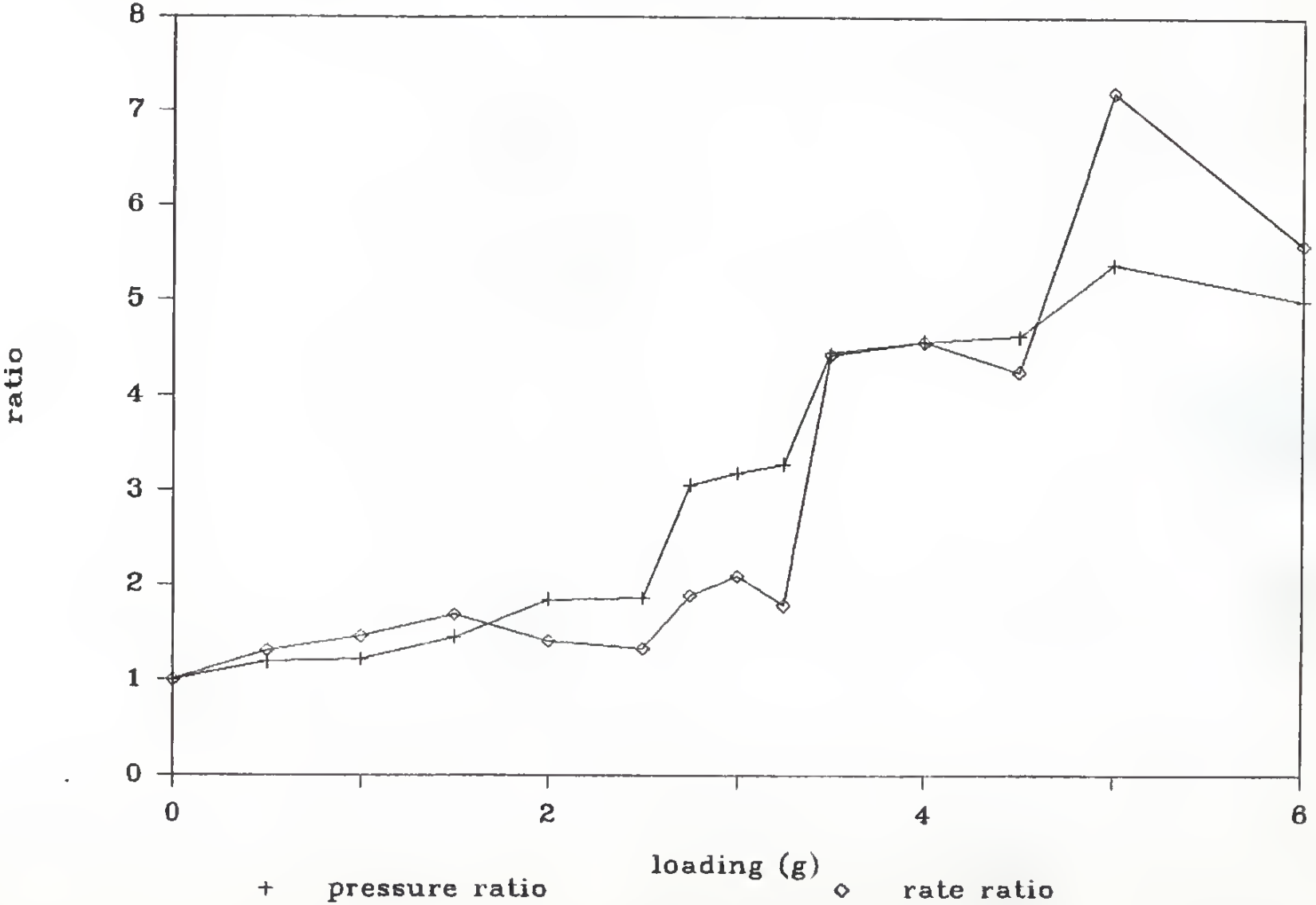
ratio
8
7
6
5
4
3
2
1
0
0
2
4
6
loading (g)
+ pressure ratio
◇ rate ratio

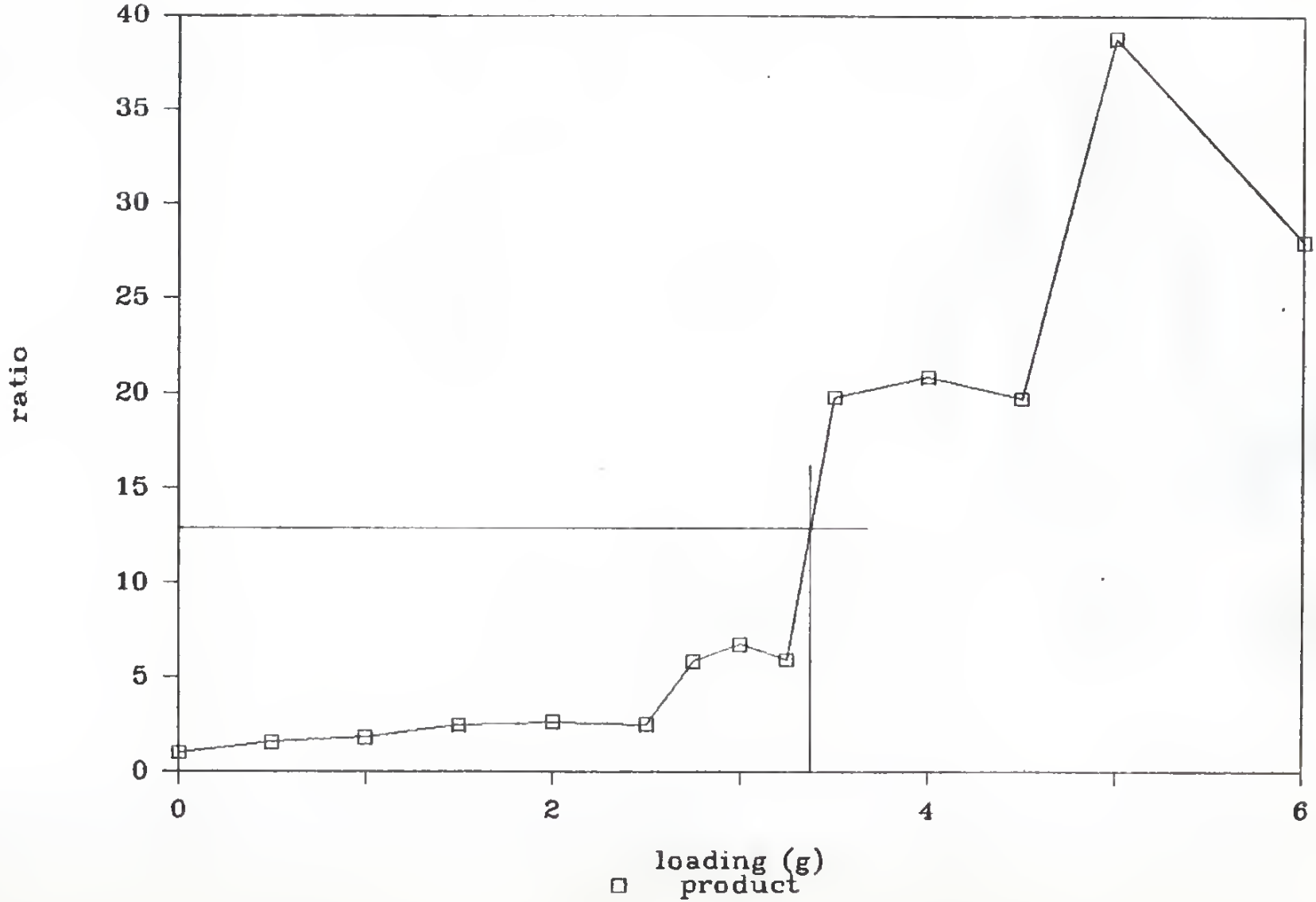
40
35
30
25
20
15
10
5
0
ratio
0
2
4
6
loading (g)
product

FIGURE 17a

Sweep of loadings for potato starch showing both the pressure ratio and the rate ratio.

FIGURE 17b

Sweep of loadings for potato starch showing the product of the pressure ratio and the rate ratio.

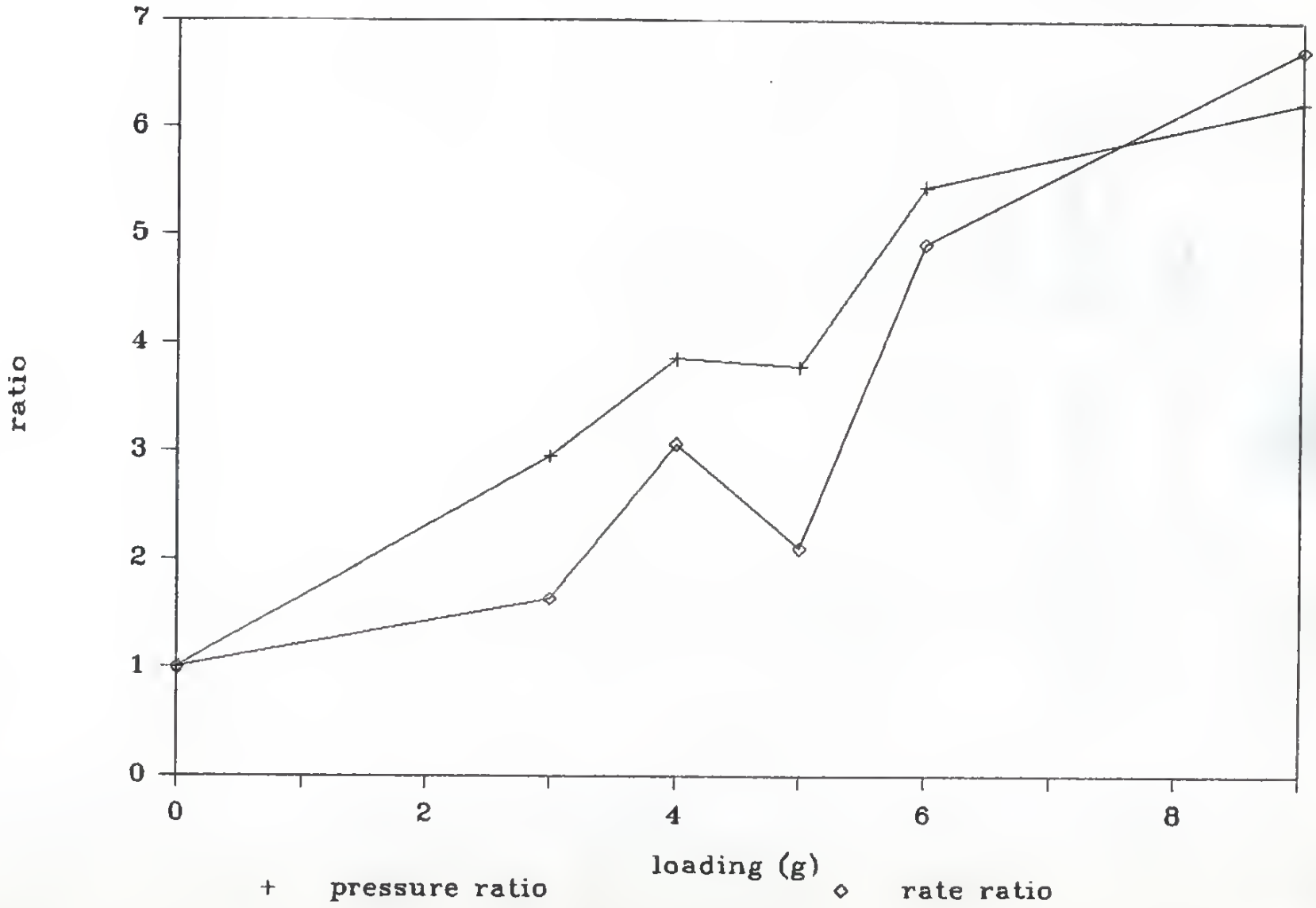
ratio
7
6
5
4
3
2
1
0
0
2
4
6
8
loading (g)
+ pressure ratio
◇ rate ratio

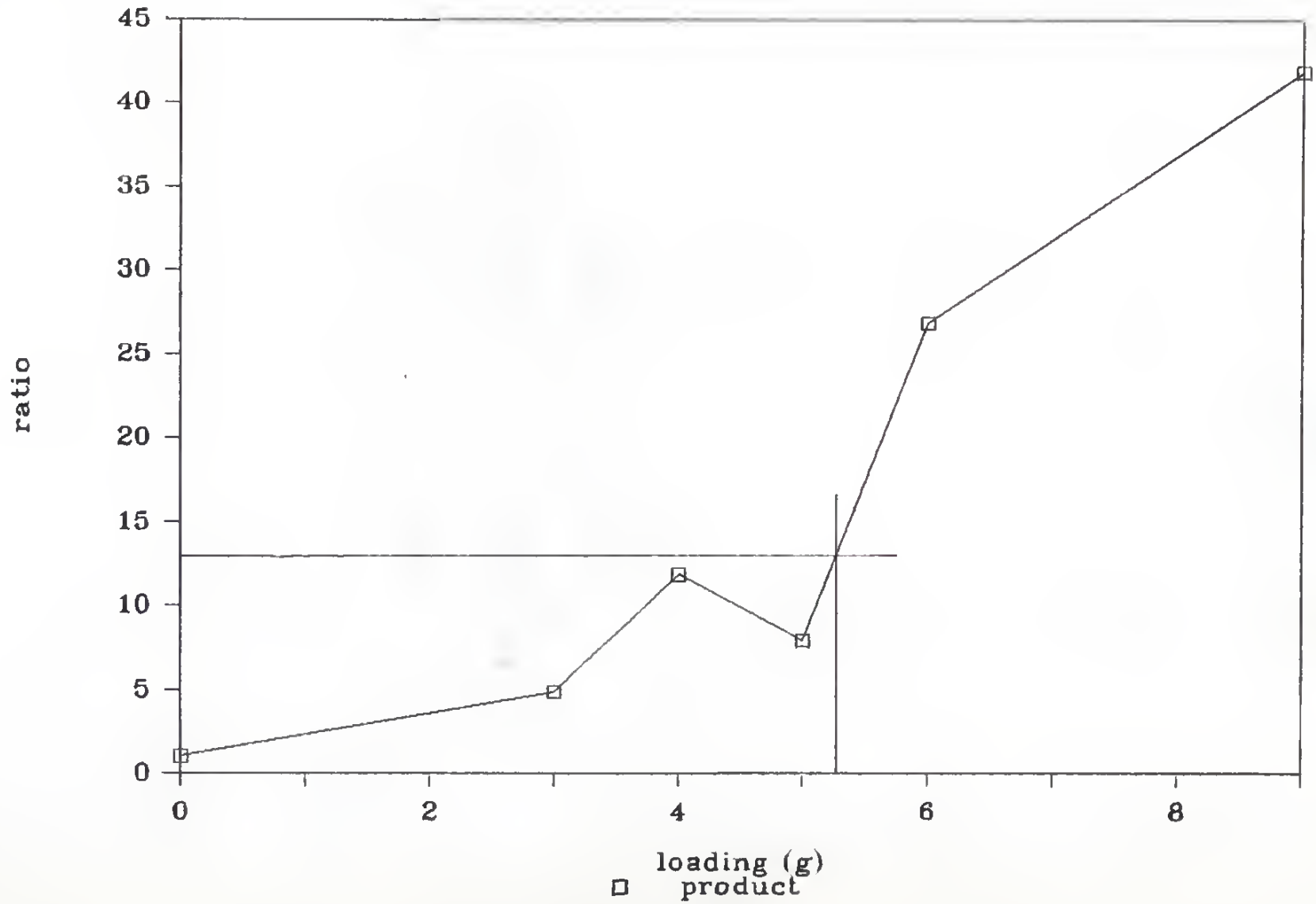
45
40
35
30
25
20
15
10
5
0
ratio
0
2
4
6
8
loading (g)
product

FIGURE 18

Plot of the product ratios produced from the delayed Robbins-Monro analysis of rice starch. The horizontal line represents the explosion threshold (R = 13) and the darkened rectangles denote explosions.

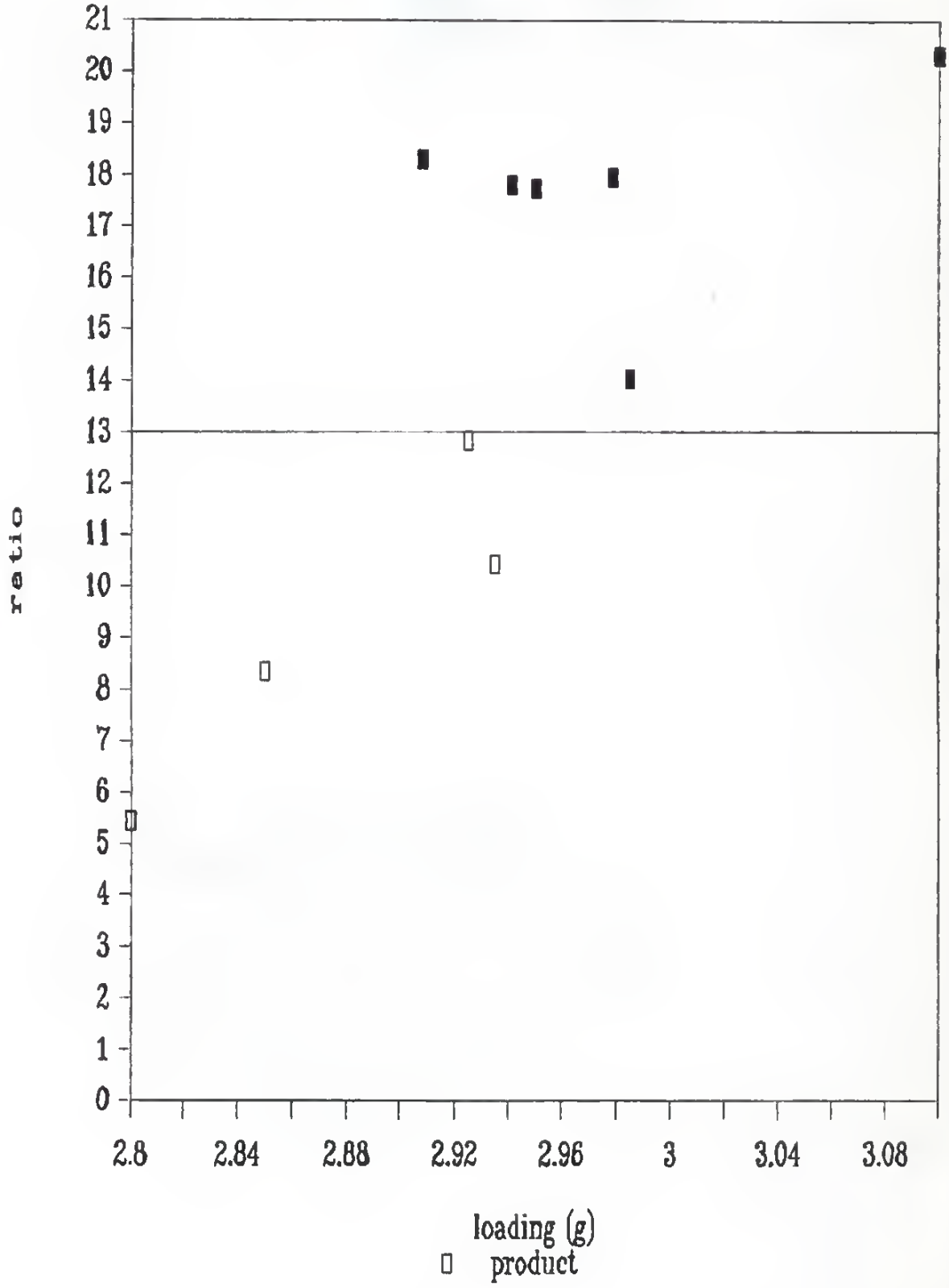
21
20
19
18
17
16
15
14
13
12
11
10
9
8
7
6
5
4
3
2
1
0
ratio
2.8
2.84
2.88
2.92
2.96
3
3.04
3.08
loading (g)
product

FIGURE 19

Plot of the product ratios produced from the delayed Robbins-Monro analysis of corn starch. The horizontal line represents the explosion threshold (R = 13) and the darkened rectanagles denote explosions.

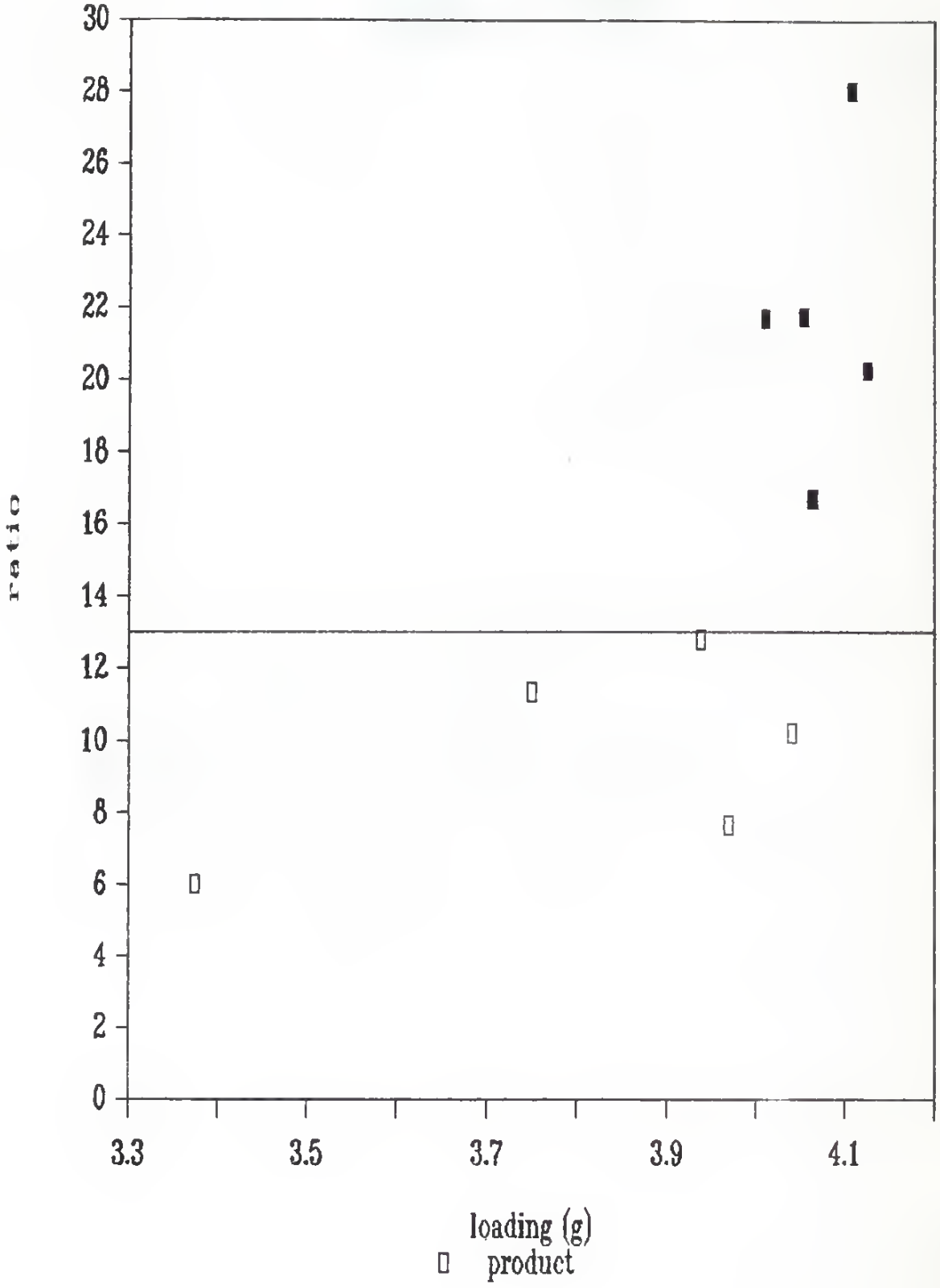
30
28
26
24
22
20
18
16
14
12
10
8
6
4
2
0
ratio
3.3
3.5
3.7
3.9
4.1
loading (g)
product

FIGURE 20

Plot of the product ratios produced from the delayed Robbins-Monro analysis of potato starch. The horizontal line represents the explosion threshold (R = 13) and the darkened rectangles denote explosions.

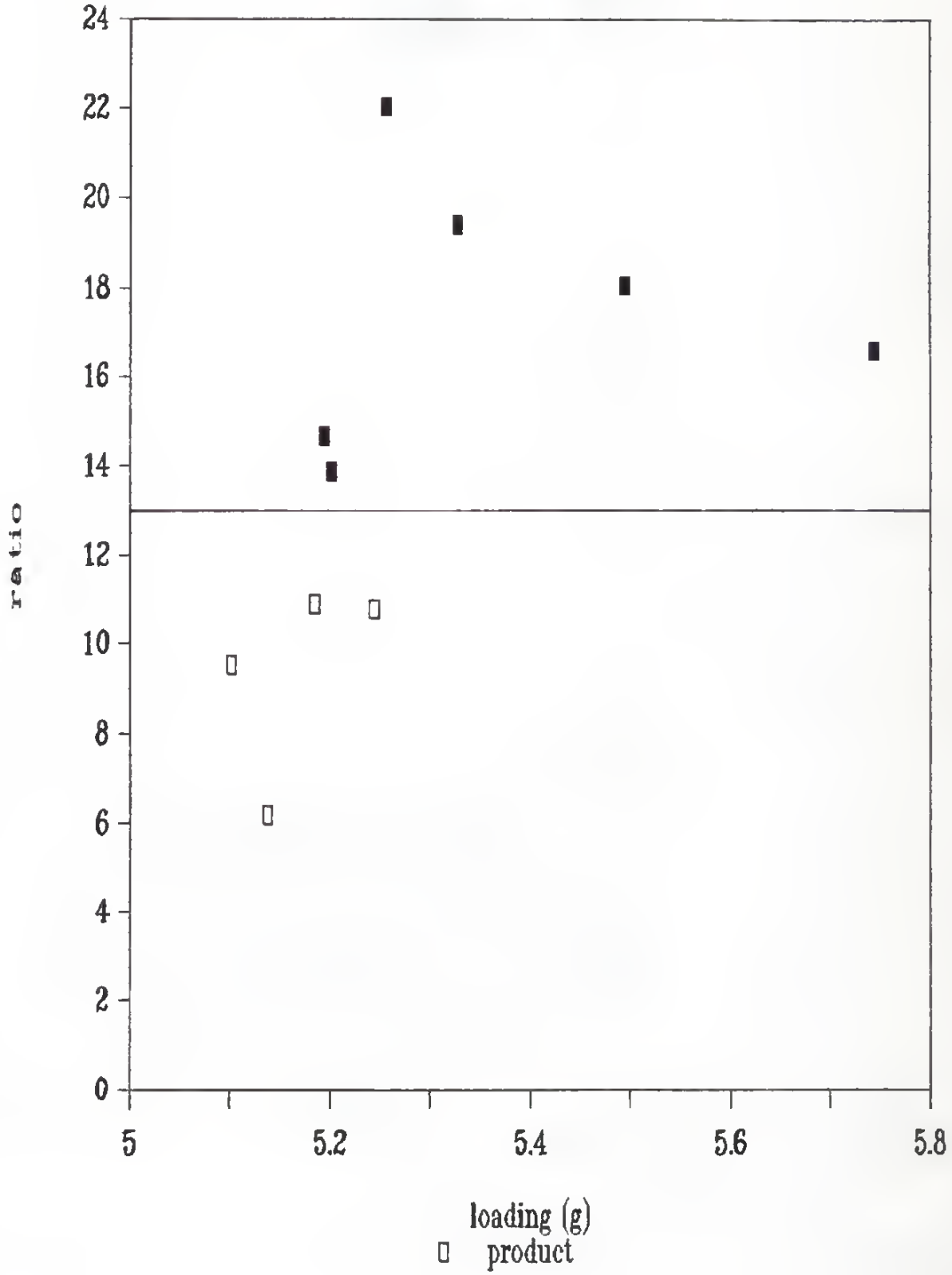
24
22
20
18
16
14
12
10
8
6
4
2
0
ratio
5
5.2
5.4
5.6
5.8
loading (g)
product

B. Particle Size Analysis

Measurements of each starch's mean particle size using three different methods are listed in Table 3. Tbe results of two metbods for rice starch indicate a firm value of 8 microns. However, there is some discrepancy between methods as tbe particle size increases. Potato starch shows a wide distribution of particle sizes. All the particle sizes measured in fluid exceed tbose measured in air (witb the exception of rice starcb which appears to retain agglomerates when dispersed into air). This is due in part to swelling of the particles wben tbey are suspended in fluid. It is tbought that the results produced by the light attenuation method may be inaccurate in part to tbe assumption made that the extinction coefficient is 2.0. As will be pointed out below in the next section, the degree to which the LED/PT system is collimated can have a strong effect upon the extinction coefficient.[19]

The results for d are also listed in Table 3. It should be noted that the d for tbe light attenuation method is arrived at directly from the Bougert-Beer-Lambert equation and no conversion (Eqn. 3.2, Appendix A) is needed.

Although some evidence for the accuracy of these measured values was gleaned from a comparison of their relative settling times when dispersed inside the 20 litre vessel, the possibility of electrical cbarging of the particles cast some doubt on the validity of assuming Stokes settling would occur.

C. Cloud Uniformity

Results of several different orientations of the light attenuation ring inside the chamber during the dispersion of 5 grams of corn starch consistently produced light attenuation traces similar to the one in Fig. 21. These trials were done without using the lens shutters and the traces begin at 100% transmittance. Particular features include the sudden decrease in transmission during the dispersion of the dust, the turbulence immediately after the dispersion, and the onset of settling. Most important however is the interval of about 30 ms occurring after the turbulence has decayed at 180 ms into the trace. Here we see that the concentration along three independent axes of the chamber is the same, and that the cloud is uniformly dispersed

As a result of these studies we have concluded that we do have a uniform cloud at least during a short interval of time and that for best results the ignition delay should be adjusted so as to ignite the cloud when it is most uniformly dispersed (at 180 ms).

D. Concentration Measurements

The dust cloud concentrations for the L.E.L. loadings of each starch as calculated from the light attenuation probes is

FIGURE 21

Typical trace of the light attenuation signals versus time for four beams: two diameter beams of the ring (perpendicular to each other), one beam along the chord, and the beam from the externally mounted probe. The zero signal represents 100% transmittance. (0% transmittance ~ 5 volts)

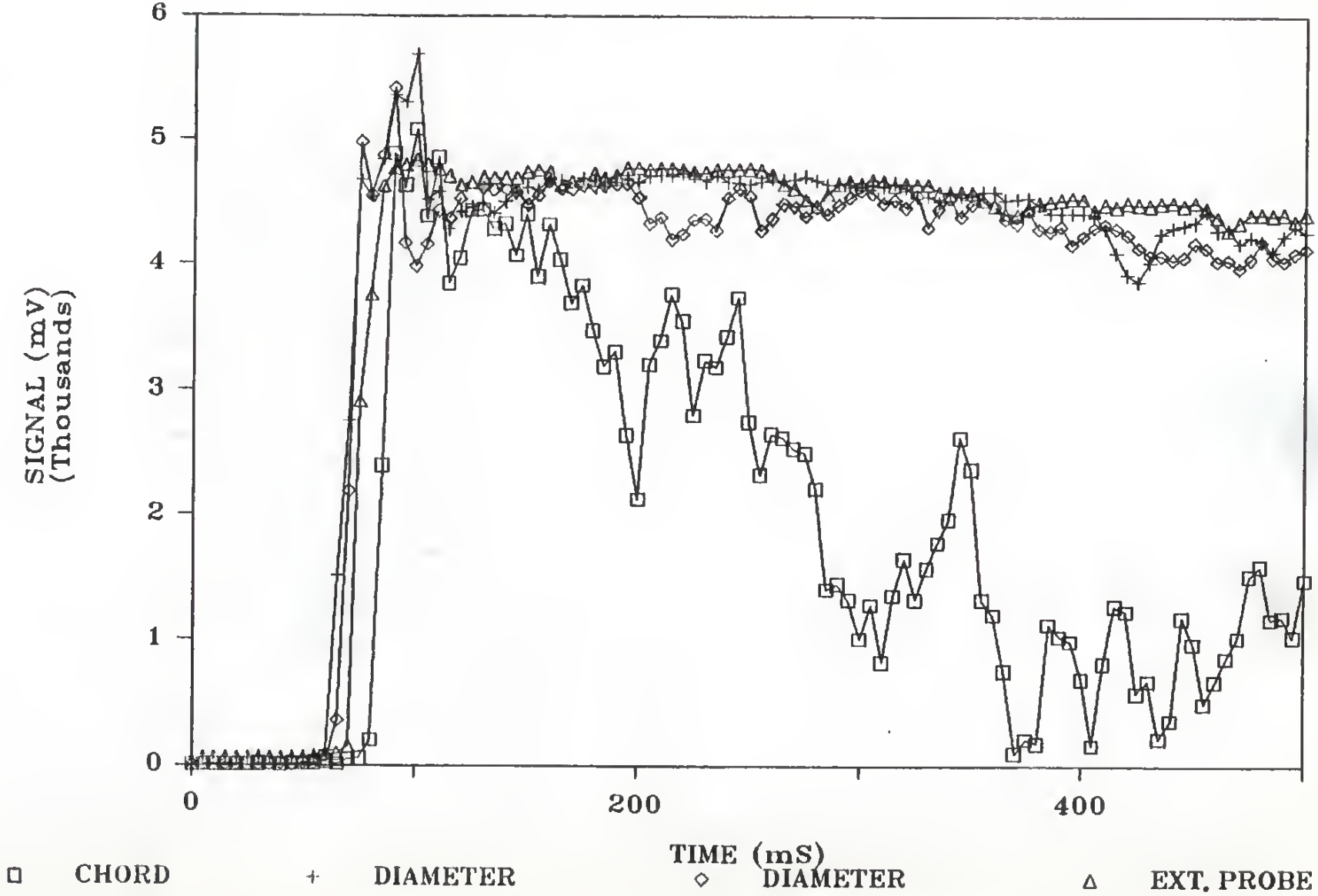
SIGNAL (mV)
(Thousands)
6
5
4
3
2
1
0
0
200
400
TIME (mS)
□ CHORD
+ DIAMETER
◇ DIAMETER
△ EXT. PROBE

presented in Table 4. Measurements were made using the light attenuation ring (diameter beams only) with shutters and the externally mounted light beam which has no shutters. Also included are the nominal concentrations based upon the loading and the chamber volume.

The concentration measurements appear reasonable, but are all significantly lower than their nominal values. The value of the L.E.L. concentration for corn starch (67 g/m^3) agrees somewhat with that arrived at by Eckhoff (43 g/m^3).[20] First, the measured values are prone to inaccuracies caused by the response of the phototransistors in the low transmission range (0% to 10% transmittance). Two of the L.E.L. concentrations produced signals in the low transmission range. In this range the signal becomes comparable to the noise and is difficult to evaluate.

There is no theoretical limit upon the length of the path through the cloud traversed by the light beam which violates the Bougert-Beer-Lambert relationship. However, there are some technical difficulties which can occur. The ability to discern the transmission signal from background electrical noise depends upon the signal to noise ratio. To increase this ratio for a given dust cloud, either the intensity of the source must be increased or the path length must be decreased. The light emitting diodes which we are using are limited in their maximum output intensity. Another option would be to improve the circuitry of the LED/PT system to include, say, an amplifier and some noise filtering.

Secondly, since the LED/PT system used was not well

collimated, due to limitations on the available space inside the chamber, the effect of collimation upon the measured concentration should be investigated.

The extinction coefficient that we chose to use (Q=2.0) has assumed that the light beam subtends zero angle (i.e. parallel beams only) and that no scattered light is received at the detector. Lothian and Chappel[21] indicate however, that the value of Q decreases as the angle subtended by the detector increases. As the angle is increased, more of the scattered light slips into the detector. Even if a light beam of zero angle could be perfected, some radiation resulting from multiple scattering could still enter the detector.

Hence, if it can be assumed that regardless of what the true extinction coefficient might be it does not vary with respect to the cloud concentration, nor vary significantly with regard to particle size within the range for which we are concerned (5 to 100 micron), then the measured concentrations should differ from the true concentration by only a constant multipling factor. Thus conclusions drawn regarding the behavior of the L.E.L. and the mean particle size should still be valid. However, it is still quite possible that the absolute values determined for the lower explosive limit are most probably underestimated and should not be considered representative of the true hazard of such a dust concentration. Consideration of the extinction curve provided by Lothian and Chappel, and the acceptance angle subtended by the phototransistors (~11°) suggest that an extinction coefficient Q=1.0 might be more appropriate. If so, then the

concentrations which have been quoted are about one-half what they should be.

The external beam produced values of the concentration which are larger than that measured by the ring. This result was expected, and is mostly due to the accumulation of dust on the lenses although the presence of the light attenuation ring placed near to the bomb wall can also alter the dust dispersion slightly.

E. Prediction of L.E.L. vs. Particle Size

With all of these possible inaccuracies noted, the results of the L.E.L. measurements of three starches indicate a dependence with respect to the mean particle size as that shown in Figs. 22,23.

This result is contingent upon improved particle size measurements and closer oomparison of other characteristics of the three starches which may cause them to differ in their ability to react explosively.

Of interest is the behavior of each dust's explosibility with regard to its ratio of surface area to volume. This ratio is proportional to $[\text{particle size}]^{-1}$. By plotting the lower explosive limit, which characterizes the explosibility, versus the reciprocal of the particle size, a 1/d dependence is apparent (Figs. 24,25).

FIGURE 22

Plot of L.E.L. vs. particle size for measurements taken with the multi-beam light attenuation probe using shutters.

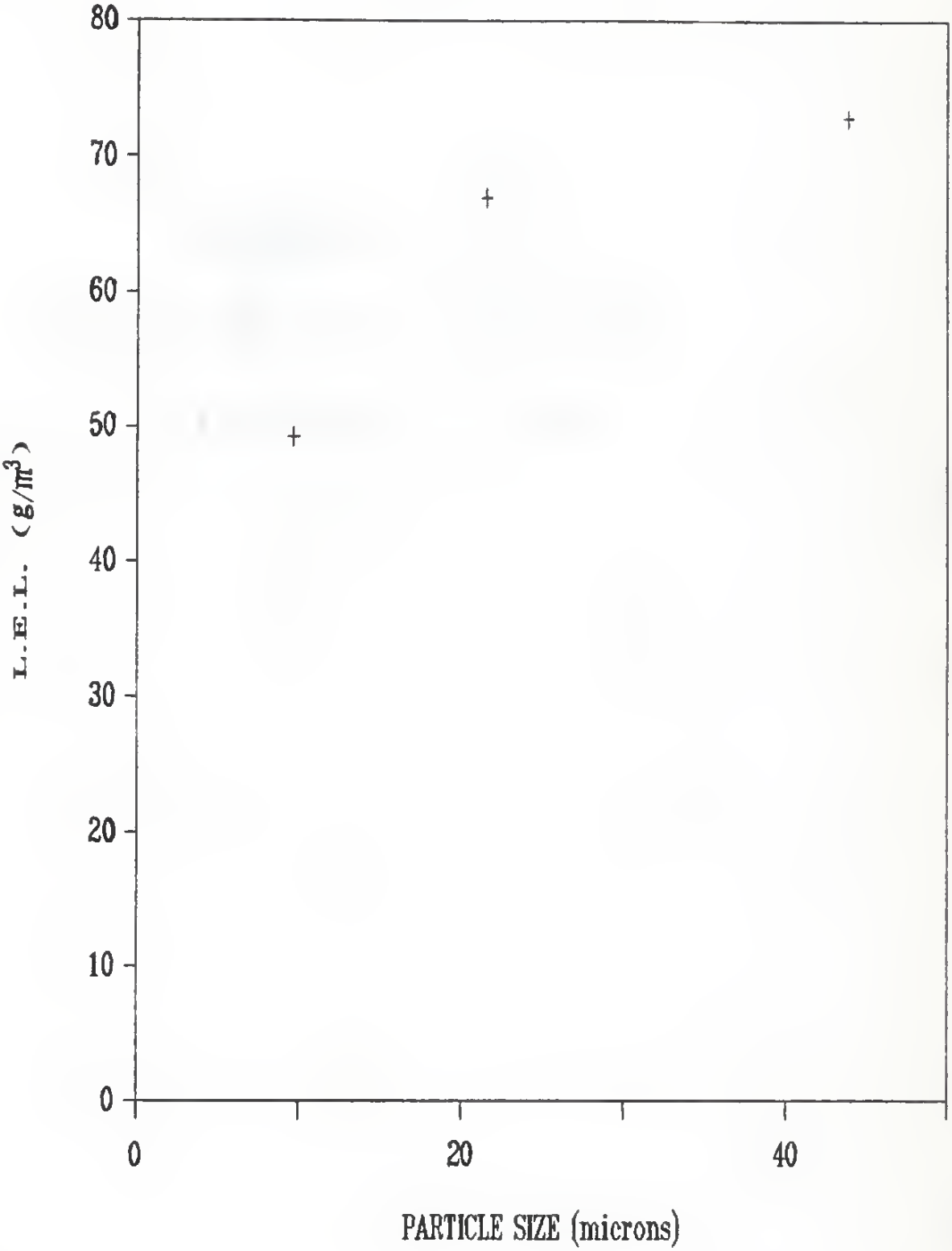
80
70
60
50
40
30
20
10
0
0
20
40
L.E.L. (g/m3)
PARTICLE SIZE (microns)

FIGURE 23

Plot of L.E.L. vs. particle size for measurements taken with the external probe using no shutters.

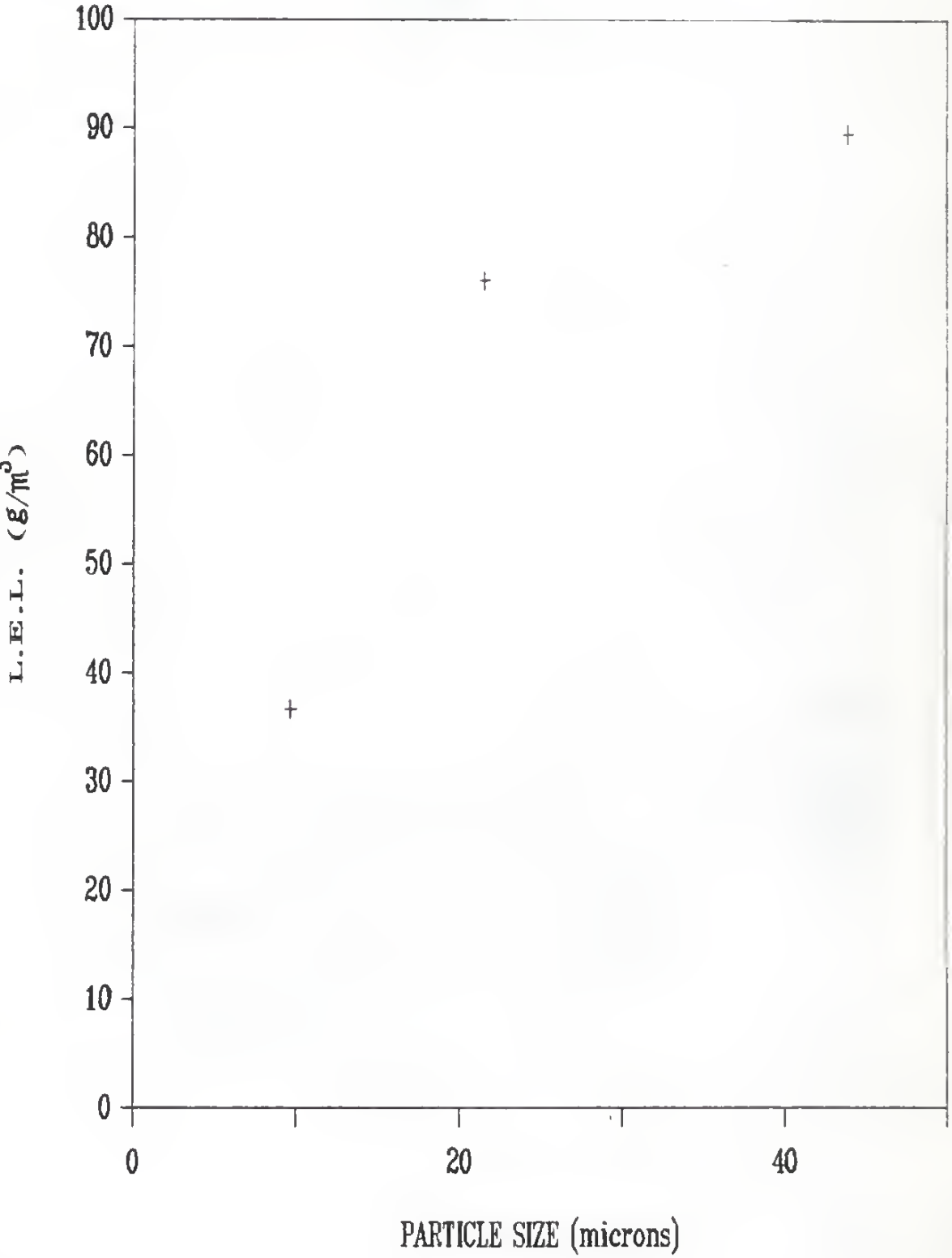
100
90
80
70
60
50
40
30
20
10
0
0
20
40
L.E.L. (g/m3)
PARTICLE SIZE (microns)

FIGURE 24

Plot of the L.E.L. vs. the reciprocal of the particle size for measurements taken with the multi-beam light attenuation probe using shutters.

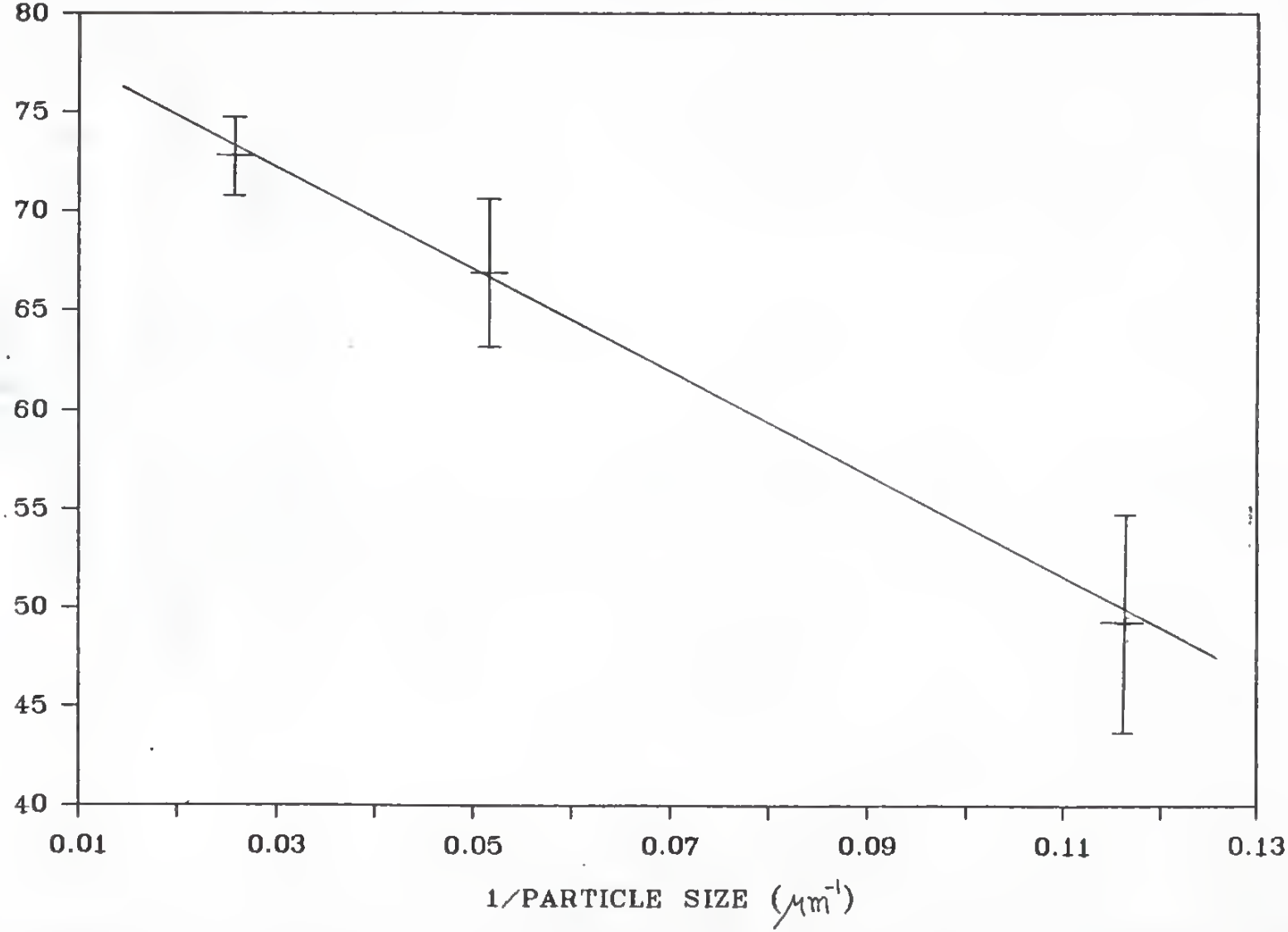
80
75
70
65
60
55
50
45
40
L.E.L. (g/m 3)
0.01
0.03
0.05
0.07
0.09
0.11
0.13
1/PARTICLE SIZE (μm-1)

FIGURE 25

Plot of the L.E.L. vs. the reciprocal of the particle size for measurements taken with the external probe using no shutters.

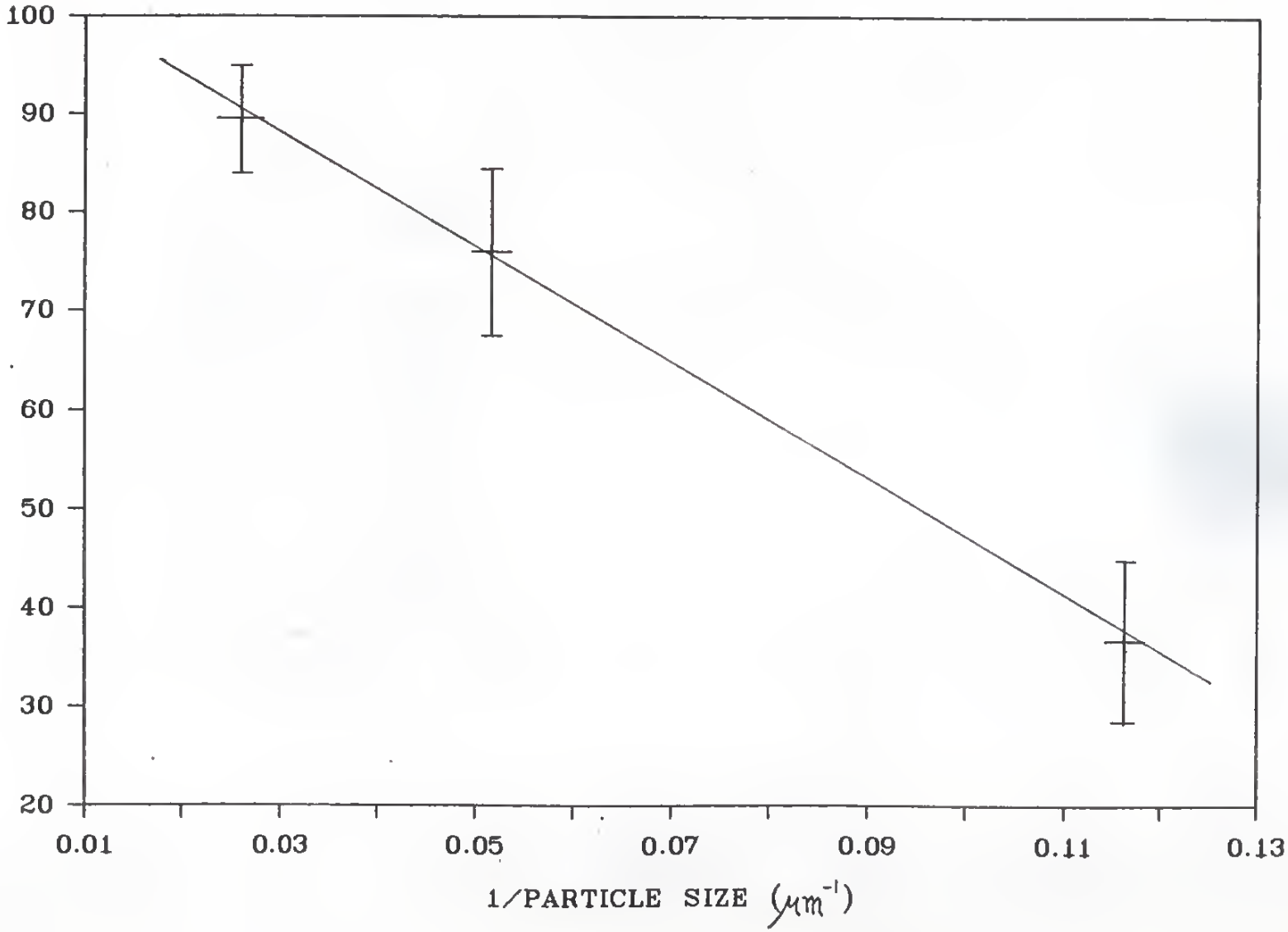
100
90
80
70
60
50
40
30
20
L.E.L. (g/m^3)
0.01
0.03
0.05
0.07
0.09
0.11
0.13
1/PARTICLE SIZE (μm^{-1})

SUMMARY

Some of the essentials of a L.E.L. measurement include characterization of the cloud uniformity, use of an accurate technique for determining the threshold concentration, and a means for accurate concentration measurements. In this work, we have studied the cloud uniformity using the attenuation of light along various paths during the development of the cloud. We have implemented statistical analysis to justify that threshold at which the L.E.L. occurs. The L.E.L.'s of three starches of well-defined particle size have been measured using a light attenuation teachnique. And, although some difficulties were experienced, it is felt that this method of concentration measurement is superior since it is both time-resolved and non-destructive.

Further, any analysis of the behavior of the L.E.L. with respect to the dust's mean particle size will require an accurate particle size measurement. In this work, the particle sizes were measured using three dissimilar methods and revealed similar results. This provides a good deal of confidence in the quoted sizes.

TABLE 1a

Preliminary sweep of loadings for rice starch with initial estimate of the L.E.L. loading.

TABLE 1b

Preliminary sweep of loadings for corn starch with initial estimate of the L.E.L. loading.

TABLE 1c

Preliminary sweep of loadings for potato starch with initial estimate of the L.E.L. loading.

PRELIMINARY SWEEP OF LOADINGS

RICE STARCH

LOAD (g)	PRESSURE (bar)	RATE (V/s)	PRESSURE RATIO	RATE RATIO	PRODUCT RATIO
0.000	0.94	3.9	1.000	1.000	1.000
1.000	1.38	5.8	1.468	1.487	2.183
2.000	2.18	5.8	2.319	1.487	3.449
2.333	3.09	9.2	3.287	2.359	7.755
2.667	3.34	8.6	3.553	2.205	7.835
3.000	4.22	16.2	4.489	4.154	18.648
4.000	5.07	32.0	5.394	8.205	44.255
5.000	6.18	72.8	6.574	18.667	122.723
6.000	7.26	90.4	7.723	23.179	179.025
7.000	7.94	115.6	8.447	29.641	250.372

The first estimate of the lower explosive limit loading is selected as 2.800 g. The step size is selected as 0.300 g.

PRELIMINARY SWEEP OF LOADINGS

CORN STARCH

LOAD (g)	PRESSURE (bar)	RATE (V/s)	PRESSURE RATIO	RATE RATIO	PRODUCT RATIO
0.000	0.94	3.9	1.000	1.000	1.000
0.500	1.12	5.1	1.191	1.308	1.558
1.000	1.15	5.7	1.223	1.462	1.788
1.500	1.37	6.6	1.457	1.692	2.466
2.000	1.74	5.5	1.851	1.410	2.610
2.500	1.76	5.2	1.872	1.333	2.496
2.750	2.88	7.4	3.064	1.897	5.813
3.000	3.00	8.2	3.191	2.103	6.710
3.250	3.09	7.0	3.287	1.795	5.900
3.500	4.19	17.3	4.457	4.436	19.773
4.000	4.30	17.8	4.574	4.564	20.878
4.500	4.35	16.6	4.628	4.256	19.697
5.000	5.06	28.1	5.383	7.205	38.785
6.000	4.71	21.8	5.011	5.590	28.008

The first estimate of the lower explosive limit loading is selected as 3.375 g. The step size is selected as 0.375 g.

PRELIMINARY SWEEP OF LOADINGS

POTATO STARCH

LOAD (g)	PRESSURE (bar)	RATE (V/s)	PRESSURE RATIO	RATE RATIO	PRODUCT RATIO
0.000	0.94	3.9	1.000	1.000	1.000
3.000	2.78	6.4	2.957	1.641	4.853
4.000	3.63	12.0	3.862	3.077	11.882
5.000	3.56	8.2	3.787	2.103	7.963
6.000	5.13	19.2	5.457	4.923	26.867
9.000	5.86	26.2	6.234	6.718	41.880

The first estimate of the lower explosive limit loading is selected as 5.244 g. The step size is selected as 0.500 g.

TABLE 2a

Results of the delayed Robbins-Monro analysis and determination of the L.E.L. loading for rice starch.

TABLE 2b

Results of the delayed Robbins-Monro analysis and determination of the L.E.L. loading for corn starch.

TABLE 2c

Results of the delayed Robbins-Monro analysis and determination of the L.E.L. loading for potato starch.

DELAYED ROBBINS-MONRO RESULTS

RICE STARCH

TRIAL	LOAD (g)	PRESSURE (bar)	RATE (V/s)	PRESSURE RATIO	RATE RATIO	PRODUCT RATIO	RESULT
1	2.800	2.93	6.8	3.117	1.744	5.435	no go
2	3.100	4.28	17.4	4.553	4.462	20.314	go
3	2.950	4.17	15.6	4.436	4.000	17.745	go
4	2 850	3.56	8.6	3.787	2.205	8.351	no go
5	2.925	3.92	12.0	4.170	3.077	12.831	no go
6	2.985	4.15	12.4	4.415	3.179	14.037	go
7	2.935	3.90	9.8	4.149	2.513	10.426	no go
8	2.978	4.22	15.6	4.489	4.000	17.957	go
9	2.941	4.19	15.6	4.457	4.000	17.830	go
10	2.908	4.30	15.6	4.574	4.000	18.298	go

Lower explosive limit loading = 2.927 g.

DELAYED ROBBINS-MONRO RESULTS

CORN STARCH

TRIAL	LOAD (g)	PRESSURE (bar)	RATE (V/s)	PRESSURE RATIO	RATE RATIO	PRODUCT RATIO	RESULT
1	3.375	3.06	7.2	3.255	1.846	6.010	no go
2	3.750	3.66	11.4	3.894	2.923	11.381	no go
3	4.125	4.32	17.2	4.596	4.410	20.268	go
4	3.938	3.98	11.8	4.234	3.026	12.811	no go
5	4.063	3.83	16.0	4.074	4.103	16.716	go
6	3.969	3.35	8.4	3.564	2.154	7.676	no go
7	4.040	3.75	10.0	3.989	2.564	10.229	no go
8	4.107	4.59	22.4	4.883	5.744	28.046	go
9	4.053	4.29	18.6	4.564	4.769	21.766	go
10	4.010	4.28	18.6	4.553	4.769	21.715	go

Lower explosive limit loading = 4.037 g.

DELAYED ROBBINS-MONRO RESULTS

POTATO STARCH

TRIAL	LOAD (g)	PRESSURE (bar)	RATE (V/s)	PRESSURE RATIO	RATE RATIO	PRODUCT RATIO	RESULT
1	5.244	3.80	10.4	4.053	2.667	10.780	no go
2	5.744	4.61	13.2	4.904	3.385	16.599	go
3	5.494	4.60	14.4	4.894	3.692	18.069	go
4	5.327	4.45	16.0	4.734	4.103	19.422	go
5	5.202	4.17	12.2	4.436	3.128	13.877	go
6	5.102	3.72	9.4	3.957	2.410	9.538	no go
7	5.185	4.08	9.8	4.340	2.513	10.907	no go
8	5.256	4.54	17.8	4.830	4.564	22.044	go
9	5.194	4.14	13.0	4.404	3.333	14.681	go
10	5.138	3.33	6.8	3.543	1.744	6.177	no go

Lower explosive limit loading = 5.209 g.

TABLE 3

Results of particle size measurements using three separate techniques: 1) HIAC in isopropyl alcohol, 2) HIAC in air, and 3) light attenuation. Definitions of d and $d_{g,m}$ are provided in appendix A.

PARTICLE SIZE ANALYSIS

HIAC in Alcohol

	$d_{g,m}$				d		
	max.	min.	ave.	s.d.	max.	min.	ave.
RICE	9.82	9.46	9.65	1.62	8.7	8.4	8.6
CORN	21.61	21.52	21.56	1.58	19.5	19.4	19.4
POTATO	46.39	41.60	43.90	1.65	40.4	37.3	38.8

HIAC in Air

	$d_{g,m}$				d		
	max.	min.	ave.	s.d.	max.	min.	ave.
RICE	32.09	17.64	24.87	1.83	27.5	14.3	19.4
CORN	23.07	17.81	20.44	1.53	20.8	16.5	18.5
POTATO	51.26	42.94	47.09	1.59	46.3	38.9	43.8

Light Attenuation

	d			
	max.	min.	ave.	s.d.
RICE	8.87	8.07	8.47	0.32
CORN	26.48	21.72	24.91	1.71
POTATO	58.40	44.67	52.33	7.00

All values are expressed in microns.

TABLE 4

Lower explosive limits as determined by measurements using both the multi-beam probe (with shutters) and the external probe (without shutters).

LOWER EXPLOSIVE LIMITS

MULTI-BEAM LIGHT ATTENUATION PROBE with SHUTTERS

STARCH	SIZE (μm)	DENSITY (g/cc)	MOISTURE (% wt)	LOADING (g)	L.E.L. (g/m^3)	NOMINAL CONC. (g/m^3)
RICE	8.59	1.548	3.54	2.927	49.23	151.35
CORN	19.40	1.535	7.69	4.037	66.90	208.75
POTATO	38.76	1.539	9.85	5.209	72.83	269.35

EXTERNAL PROBE

STARCH	SIZE (μm)	DENSITY (g/cc)	MOISTURE (% wt)	LOADING (g)	L.E.L. (g/m^3)	NOMINAL CONC. (g/m^3)
RICE	8.59	1.548	3.54	2.927	36.67	151.35
CORN	19.40	1.535	7.69	4.037	76.04	208.75
POTATO	38.76	1.539	9.85	5.209	89.54	269.35

REFERENCES

1. **Kameyama**, Y., Lai, F.S., Sayama, H., Fan, L.T., "The Risk of Dust Explosions in Grain Processing and Handling Facilities," Journal of Agricultural Engineering Research, **27**:253-259, 1982.

2. **Griffith**, W.C., "Dust Explosions," Ann. Rev. Fluid Mech., **10**:93-105, 1978.

3. **Oppenheim**, A.K. and Soloukhin, R.I., "Experiments in Gasdynamics of Explosions," Ann. Rev. Fluid Mech., **5**:31-51, 1973.

4. **Hertzberg**, M., Cashdollar, K.L., Opferman, John J., "The Flammability of Coal Dust-Air Mixtures: Lean Limits, Flame Temperatures, Ignition Energies, and Particle Size Effects," Bureau of Mines Report of Investigations, RI 8360, 1979.

5. **Eggleston**, Lester A. and Pryor, Andrew J., "The Limits of Dust Explosibility," Fire Technology, **3**(2):77-78, May 1967.

6. **Cashdollar**, K.L. and Hertzberg, M., "20-l Explosibility Test Chamber for Dusts and Gases," Rev. Sci. Instrum., **56**(4):596-602, April 1985.

7. **Eckhoff**, Rolf K., "Experimental Determination of Minimum Explosive Dust Concentration: an outline of the problem and a sketch of a possible apparatus for routine tests," The Chrs. Michelsen Institute, report no. CMI 77005-1, May 1977.

8. **Martin**, C.R., Aldis, D.F., Lee, R.S., "IN SITU Measurement of Grain Dust Particle Size Distribution and Concentration," American Society of Agricultural Engineers winter meeting, Paper no. 80-3561, 1980.

9. **Toong**, Tau-Yi, Combustion Dynamics: The Dynamics of Chemically Reacting Fluids, McGraw-Hill, 1983.

10. **Mitsui**, R. and Tanaka, T., "Simple Models of Dust Explosion. Predicting Ignition Temperature and Minimum Explosive Limit in Terms of Particle Size," Industrial and Engineering Chemistry, Process Development and Design, **12**:384-389, 1973.

11. **Hartman**, I. and Nagy, J., U.S. Bureau of Mines, Information Circular No. 3751, p. 38, 1944.

12. Cassel, H.M. and Liebman, I., Combustion and Flame, 3:467-475, 1959.

13. Nagy, J., Conn, John W., and Verakis, H.C., "Explosion Development in a Spherical vessel," U.S. Department of the Interior, Bureau of Mines, Report of Investigations, RI-7279, 1969.

14. Bradley, D. and Mitcheson, A., "Mathematical Solutions for Explosions in Spherical Vessels," Combustion and Flame, 26:201-207, 1976.

15. Kerker, M., The Scattering of Light and Other Electromagnetic Radiation, Chap. 4, Academic Press, NY, NY; 1969.

16. Davis, Miles, "Comparison of Sequential Bioassays in Small Samples," Journal of the Royal Statistical Society, Series B, 33:78-87, 1971.

17. Liebman, I., Conti, R.S. and Cashdollar, K.L., "Dust Cloud Concentration Probe," Rev. Sci. Instrum., 48:1314-1316, 1977.

18. American Association of Cereal Chemists. Approved method of the AACC, Method 44-01 approved Oct. 1975; The Association: St. Paul, MN., 1976.

19. Martin, C.R., 1985. Personal communication.

20. Eckhoff, Rolf K., "A New Laboratory-Scale Method for Determining the Minimum Explosible Concentration of Dust Clouds," The Chrs. Michelsen Institute, report no. CMI 77005-2, April 1978.

21. Lothian, G.F. and Chappel, F.P., "The Transmission of Light Through Suspensions," J. appl. Chem, 1:475-482, November, 1951.

22. Stookham, J.D. and Fochtman, E.G., Particle Size Analysis, Ann Arbor Science Publishers Inc., Ann Arbor, Mich.; 1977.

HIAC MEASUREMENT of PARTICLE SIZE DISTRIBUTION

CALIBRATION

Divide a range of diameters from lower limit to upper limit into i geometric progressions such that:

$$D_i = D_o k^i$$

$$k = \exp[(1/i)\ln(D_i/D_o)] \qquad (1.1)$$

where:

D_i = upper limit diameter

D_o = lower limit diameter

k = geometric progression constant

Then the particle threshold diameter for the n^{th} progression becomes:

$$D_n = D_o k^n \qquad (1.2)$$

and

$$D_u = D_i \quad \text{for } n = i$$

$$D_l = D_o \quad \text{for } n = 0$$

Set the thresholds of the i HIAC channels (i=5 for model PC 305) for pulse amplitude as determined by:

$$E_p = \pi D^2 E_b / 4S^2$$

where:

E_p = pulse amplitude from photodetector

D = diameter of calibration particle

S = side of square window

E_b = 10 volts base output from photodetector

now,

$$E_p = 7.85 \ (D^2/S^2) \qquad (2.1)$$

and for sensors,

2-60 micron range $E_p = 2.18 \times 10^{-3} D^2$

5-150 micron range $E_p = 3.49 \times 10^{-4} D^2$

DATA ANALYSIS

From the geometric progression established by calibration, the geometric progression ratio for the n^{th} progression to the first progression is:

$$R^m_n = D^m_n / D^m_1$$

where

m = moment of the geometric progression

= 1, for number

= 2, for area

= 3, for volume

and from (1.2)

$$R^m_n = (D_1 k^n)^m / (D_1 k^1)^m$$

$$R^m_n = k^{m(n-1)} \qquad (3.1)$$

From the numeric progression data of particles measured by the HIAC, the relative (ratio) magnitude of particle moment in progression n is

$$M^m_n = N_n R^m_n$$

where

N_n = number of particles in progression n

The percent of the geometric progression magnitude in progression n would be

$$\%^m_n = \{M^m_n / \text{sum of all } M^m_n\} \times 100\%$$

Thus, for a given moment, the geometric cumulative distribution with respect to particle diameter was calculated as:

$$\text{Cumulative } \%^m_n > D_n = \%^m_i + \%^m_{i-1} + \ldots + \%^m_1$$

where

$$\%m_1 = 100$$

and the parameters of a lognormal probability distribution $d_{g,m}$ and s.d. (Stocklawn and Footman 1977)[22] were calculated by regression analysis. For calculating dust cloud concentration from light transmission data,

$$d = d^3_{a,3}/d^2_{a,2} = d_{g,m} \exp\{-.5\ [\ln(s.d.)]^2\} \qquad (3.2)$$

where,

$d_{g,m}$ = geometric mass mean particle size

$d_{a,3}$ = arithmetic volume mean particle size

$d_{a,2}$ = arithmetic surface mean particle size

PROCEDURE

In Alcohol

The particles were kept suspended in isopropyl alcohol during analysis by stirring. Rice starch was dispersed during one minute of ultrasonic agitation. Corn and potato starch were dispersed by stirring.

The flow rate was determined by timing the flow of a measured volume of alcohol and a concentration of sample particles was established that did not exceed the sensor limit for coincidence.

The sensor range was selected so as to produce a maximum particle count in the middle channel.

Three or more replications were made after a one minute measurement.

In Air

Small samples of each starch were placed at the base of the modified Hartmann chamber and were dispersed by a 15 p.s.i. blast of air.

Sample concentrations were choosen so as not to exceed the sensor limit for coincidence.

The sensor range was selected so as to produce a maximum particle count in the middle channel.

Three or more replications were made.

MEASUREMENT OF THE LOWER EXPLOSIVE LIMIT OF COMBUSTIBLE DUST CLOUDS IN A 20-LITRE SPHERICAL CHAMBER

by

DAVID LEE SIDEBOTTOM

B.S., Kansas State University, 1983

AN ABSTRACT OF A MASTER'S THESIS

submitted in partial fulfillment of the

requirements for the degree

MASTER OF SCIENCE

Department of Physics

KANSAS STATE UNIVERSITY
Manhattan, Kansas

1985

ABSTRACT

Explosion studies were carried out on three starches using a 20-litre spherical explosion chamber. The dusts were dispersed with a blast of high-pressure air and the resulting dust clouds were characterised *in situ* by simultaneously measuring the attenuation of light beams along several optical paths inside the chamber. the clouds were ignited with a high-energy chemical igniter and explosions were detected and characterised with piezoelectric quartz pressure transducers. The behavior of the lower explosive limit with respect to the mean particle size of the dust was determined and indicates that the explosibility of a dust is related to the ratio of its surface area to its volume.